



Published in final edited form as:

Neuron. 2022 October 19; 110(20): 3374–3388.e8. doi:10.1016/j.neuron.2022.08.001.

A Locus Coeruleus- dorsal CA1 dopaminergic circuit modulates memory linking

Ananya Chowdhury^{1,*}, Alessandro Luchetti^{1,*}, Giselle Fernandes^{1,*}, Daniel Almeida Filho¹, George Kastellakis², Alexandra Tzilivaki^{2,3,4,5}, Erica M Ramirez¹, Mary Y Tran¹, Panayiota Poirazi², Alcino J Silva^{1,6}

¹Departments of Neurobiology, Psychiatry & Biobehavioral Sciences, and Psychology, Integrative Center for Learning and Memory, and Brain Research Institute, UCLA, Los Angeles, CA 90095.

²Institute of Molecular Biology and Biotechnology, Foundation for Research and Technology, Hellas (FORTH), Vassilica Vouton, PO Box 1527, GR 711 10 Heraklion, Crete, Greece.

³Charité – Universitätsmedizin Berlin, corporate member of Freie Universität Berlin, Humboldt-Universität zu Berlin, and Berlin Institute of Health Charitéplatz 1, 10117 Berlin Germany

⁴Einstein Center for Neurosciences Berlin Charitéplatz 1, 10117 Berlin Germany

⁵Neurocure Cluster of Excellence Charitéplatz 1, 10117 Berlin, Germany

⁶Lead contact

Summary

Individual memories are often linked so that the recall of one triggers the recall of another. For example, contextual memories acquired close in time can be linked, and this is known to depend on a temporary increase in excitability that drives the overlap between dorsal CA1 (dCA1) hippocampal ensembles that encodes the linked memories. Here, we show that Locus Coeruleus (LC) cells projecting to dCA1 have a key permissive role in contextual memory linking, without affecting contextual memory formation, and that this effect is mediated by dopamine. Additionally, we found that LC to dCA1 projecting neurons modulate the excitability of dCA1 neurons, and the extent of overlap between dCA1 memory ensembles, as well as the stability of coactivity patterns within these ensembles. This discovery of a neuromodulatory system that specifically affects memory linking without affecting memory formation, reveals a fundamental separation between the brain mechanisms modulating these two distinct processes.

Correspondence: silvaa@mednet.ucla.edu, ananyachowdhury@mednet.ucla.edu.

*These authors contributed equally.

Author contributions: A.C., A.L., G.F., D.A.F. and A.J.S. contributed to the study design. A.C. designed, and performed the LC experiments with support from A.L., E.R. and M.T. A.L. designed and performed RN experiments. A.L. performed analyses of the miniscope experiments with support from D.A.F. and A.C. Electrophysiological experiments were designed and performed by G.F. with support from A.C. and A.L. D.A.F. and A.L. wrote the code used for miniscope analyses. G.K., A.T. and P.P. designed and implemented the neurocomputational model. A.C. and A.J.S. conceptualized the study and wrote the paper together with all the other authors.

Competing interests: The authors declare no competing interests.

Keywords

Contextual Memory; Memory Linking; Neuromodulation; Locus Coeruleus; Dorsal Hippocampus; Ensembles; Dopamine

Introduction

Most memories are organized into structures, and time is one of the factors underlying their organization (Cai et al., 2016; Chowdhury and Caroni, 2018; de Sousa et al., 2021; Rashid et al., 2016; Sehgal et al., 2018; Silva et al., 2009). For example, contextual memories encoded close in time (hours, but not days) are linked such that recall of one memory triggers the recall of others acquired within the same temporal window (Cai *et al.*, 2016; Rashid *et al.*, 2016). Furthermore, previous studies showed that the overlap between contextual memory ensembles in hippocampal dorsal CA1 (dCA1) is greater when contextual memories are linked than when they are not (Cai *et al.*, 2016). Any given span of time can include many different events, only some of which may be worth remembering and linking to pre-existing memories. Indeed, there are neuromodulatory systems that use saliency, novelty, and reward to affect the strength of individual memories, and we propose that one or more of these systems may also signal when memory linking should take place. Indiscriminate or inappropriate linking of information may contribute to cognitive deficits associated with neuropsychiatric disorders, including schizophrenia, depression, and posttraumatic stress disorders (Avery et al., 2019; Jung and Lee, 2016; Nemeth et al., 2016; Titone et al., 2004).

While CREB activation and subsequent increases in neuronal excitability are thought to trigger the molecular and cellular cascades that lead to memory linking (Han et al., 2009; Rashid *et al.*, 2016; Sano et al., 2014; Zhou et al., 2009), it is not known whether there are neuromodulatory mechanisms that specifically regulate memory linking. Neuromodulatory systems have been shown to affect very specific aspects of behavior, including learning, memory, reward, fear, anxiety, etc. (Avery and Krichmar, 2017; Likhtik and Johansen, 2019; Sosa and Giocomo, 2021; Thiele and Bellgrove, 2018), and they could also regulate how and when memories are linked (Gonzalez et al., 2021). Furthermore, the dCA1 has been shown to receive dense projections from serotonergic Raphe Nuclei (RN) (Kocsis et al., 2006; Luchetti et al., 2020; Varga et al., 2009) and the Locus Coeruleus (LC), a major source of both noradrenaline and dopamine (Kempadoo et al., 2016; McNamara and Dupret, 2017; Poe et al., 2020; Smith and Greene, 2012; Takeuchi et al., 2016). Interestingly, although dopaminergic inputs from the VTA project heavily to the ventral CA1 (Lisman and Grace, 2005), its terminals were shown to be nearly absent in dCA1 (Kempadoo *et al.*, 2016; Takeuchi *et al.*, 2016). Dopamine has been implicated in the detection of novelty, prediction error, and long-term memory (Duszkiewicz et al., 2019; Kempadoo *et al.*, 2016; Lammel et al., 2011; Lemon and Manahan-Vaughan, 2006; Shohamy and Adcock, 2010; Takeuchi *et al.*, 2016; Wagatsuma et al., 2018). Noradrenaline and serotonin have been shown to be crucial in detecting the motivational valence and salience of an event (Cohen et al., 2015; Strange et al., 2003; Teissier et al., 2015; Ventura et al., 2008). Therefore, both the RN and the LC could potentially have a role in modulating memory linking in dCA1.

Here, we demonstrate that dopaminergic fibers from LC to dCA1 are critical for linking contextual memories acquired close in time, but they are not essential for contextual memory formation. The LC modulation of dCA1 affects neuronal excitability in this structure, and is required for the increased overlap between linked memory ensembles in dCA1, as well as for the stability of their coactivity patterns. These results reveal the existence of a neuromodulatory system that regulates the molecular, cellular and circuit mechanisms that specifically modulate memory linking.

Results

LC to dorsal CA1 projecting cells are required for contextual memory linking, but not for contextual memory formation

To investigate the involvement of the neuromodulatory areas, LC and RN, in contextual memory linking, we first quantified the percentage of TH+ and 5-HT+ cells activated by a novel context in the LC and RN respectively. 10 min of context exploration triggered a significant increase in cFos+ cells in both the LC (Fig. 1A) and RN (Suppl. Fig 1A) compared to home cage controls. Next, we tested if the cells projecting to the dorsal hippocampus (dHP) were required for contextual memory linking.

Linking or connecting memories acquired close in time organizes these memories such that attributes associated with one (e.g., fear) are also shared with the other. During recall, the two linked contexts elicit comparable freezing in mice, while a neutral novel context C triggers significantly lower freezing compared to both the A and B contexts. This confirms that the transfer of fear memory was not extended to novel contexts the mice had never experienced before (as shown with Context C), ruling out fear generalization or lack of discrimination (Cai *et al.*, 2016).

To investigate the role of LC to dCA1 projecting cells, we used an intersectional viral approach, where a retrograde canine adenovirus (CAV) expressing Cre-recombinase (Hnasko et al., 2006; Soudais et al., 2001) was stereotaxically injected into the dCA1, and AAV-hSyn-DIO-hM4D(Gi)-mCherry (experimental group) or AAV-hSyn-DIO-mCherry (control) (Armbruster et al., 2007; Krashes et al., 2011) was injected into the LC (Fig. 1B). This led to the expression of an inhibitory DREADD or mCherry control only in those LC neurons that monosynaptically project to dCA1 (Fig 1B and Suppl. Fig 2A). We used clozapine-N-oxide (CNO) in all the mice, administered 30 minutes before a 10-minute exploration of a novel context (context A), to inhibit the LC to dCA1 projecting neurons. Using this approach, we were able to significantly reduce the firing rate of LC neurons (Suppl. Fig 2B, C), and the proportion of cFos+ neurons in the LC (Suppl. Fig 2D, E), without affecting the neighboring TH+ cells that do not project to the dCA1 (Suppl. Fig 2F). We confirmed that CNO by itself did not affect cFos expression (Suppl. Fig. 3A) or exploratory behavior (Suppl. Fig 3B). Five hours later, the mice were allowed to explore a second novel context (context B), and two days later the mice received a shock immediately upon entering context B. Over the next three days, the mice were tested in context A, context B and in a third novel context (context C - neutral) to test for contextual memory linking, contextual fear conditioning, and contextual generalization, respectively (Fig 1C top). The tests were done on separate days (context B and C recall days were counterbalanced) to

minimize interference between tests. The control mice showed significantly higher freezing in both context A and the shocked context B compared to the neutral context C, (Fig. 1C bottom), demonstrating robust memory linking. Remarkably, the experimental group froze significantly less in context A compared to context B (shocked context), and freezing in context A was comparable to freezing in the neutral context C. This result demonstrates that inhibiting LC cells projecting to dCA1 during exploration of context A disrupts performance in our contextual memory linking test, without affecting fear generalization (Fig. 1C).

Since deficits in contextual memory could confound the interpretation of our memory linking results, we next tested whether suppressing LC to dCA1 cells affected contextual memory formation (Fig 1D top). The results showed that both groups of mice exhibited significantly higher freezing in the shocked context than in the novel context (Fig 1D bottom). This demonstrates that although inhibiting LC neurons projecting to dCA1 disrupts contextual memory linking, it does not affect the formation of individual contextual memories. Thus, the impairment in contextual memory linking cannot be attributed to deficits in contextual memory formation, a result that reveals the presence of a neuromodulatory mechanism that regulates the linking of two memories, distinct from neuromodulatory mechanisms that modulate the formation of single memories.

To confirm the projection-specificity of LC to dCA1, we performed two sets of additional experiments. We optogenetically inhibited the LC fibers in dCA1 using a DIO-Arch or a DIO-EYFP virus in the LC of TH-cre mice during the exploration of context A (Suppl. Fig 4A and B). In a parallel experiment, we injected CAV-cre in dCA1 and expressed a synaptically modified Gi-DREADD in these dCA1 projecting LC cells. CNO was locally infused into dCA1 through implanted cannulas 30 min before the exploration of context A to inhibit the LC fibers in dCA1 (Doron et al., 2020; Stachniak et al., 2014) (Suppl. Fig 4C and D). The results of these experiments show that specifically targeting the LC-dCA1 projections is sufficient to impair memory linking.

LC to dorsal CA3 projecting cells are required for contextual memory formation

In addition to projecting to dCA1, the LC also projects to dCA3 (Kempadoo *et al.*, 2016; Takeuchi *et al.*, 2016; Wagatsuma *et al.*, 2018). To investigate the role of LC cells projecting to dCA3 in contextual memory linking and contextual memory formation, we used the same viral approach described above, except that the retrograde CAV expressing Cre-recombinase was stereotaxically injected into dCA3 (Fig. 2A). Then, all the mice went through the same paradigm as described above (Fig. 2B top). The result demonstrates that inhibiting LC cells projecting to dCA3 disrupts performance in contextual memory linking: the mice exhibited comparable freezing in contexts A and C and significantly lower freezing than in the shocked context B (Fig. 2B bottom). However, this inhibition also impairs contextual memory formation (Fig. 2C top): The mice with DREADD-dependent inhibition of the LC to dCA3 cells had a significant reduction of freezing in the shocked context compared to the mCherry controls, and this freezing was indistinguishable from the freezing observed in the neutral context (Fig. 2C bottom). These results were consistent with recent findings showing that optogenetic inhibition of LC fibers projecting to dCA3 resulted in a deficit in contextual memory, while inhibiting LC projections to dCA1 did not (Wagatsuma *et al.*, 2018).

To determine whether the LC projections to dCA1 and dCA3 arise from separate but overlapping cell populations in LC, we injected two different retrobeads in the hippocampus of the same mouse: 488 (green fluorescent) in dCA1 and 568 (red fluorescent) in dCA3. After 3 weeks, we analyzed the colocalization of these colored beads in the LC. The results showed that out of the dCA1 projecting population of LC cells, $30.88 \pm 7.67\%$ were also dCA3 projecting, and that $69.12 \pm 7.67\%$ were exclusively projecting to dCA1. Similar proportions were observed in dCA3 projecting LC cells ($30.37 \pm 3.17\%$, $69.63 \pm 3.17\%$) (Suppl. Fig 5). This suggests that although there are LC cells that project to both areas, there are also sub-region specific connections between the LC and the hippocampus that could support their individual functions, such as contextual memory linking. Indeed, the projection specific manipulation of LC fibers in dCA1 (previous section, Suppl. Fig 4) confirms that directly inhibiting only the dCA1-LC projections is sufficient to impair memory linking without affecting contextual conditioning.

RN to dorsal CA1 projecting cells are not required for contextual memory linking

Next, we tested whether RN cells projecting to dCA1 are necessary for contextual memory linking. We used the same intersectional viral approach and linking paradigm described above with CNO administered to each mouse 30 min before exposure to context A (Suppl. Fig 1B and C top). Both groups of mice showed significantly higher freezing in context A and B than in the neutral context C (Suppl. Fig 1C bottom), demonstrating robust contextual memory linking. This result shows that inhibiting RN cells projecting to dCA1 does not impair contextual memory linking. To confirm whether the chemogenetic approach did indeed affect RN cells projecting to dCA1, we checked cFos expression in RN upon exploration while inhibited (Suppl. Fig 1D top). We showed that cFos was reduced in the Gi-mCherry expressing cells of RN projecting to dCA1 compared to the mCherry controls (Suppl. Fig 1D bottom). This suggests that although RN is activated by novel exploration (Suppl. Fig 1A), and the Gi-DREADD suppresses the activity of the cells projecting to dCA1, they do not affect memory linking when inhibited during the acquisition of the first context, a time when inhibition LC cells projecting to dCA1 disrupted memory linking.

All together the results presented above indicate that while LC to dCA1 projecting neurons are specifically involved in contextual memory linking, LC to dCA3 projecting neurons are required for contextual memory formation, and RN cells projecting to dCA1 are not required for either of these two processes. These findings reveal that memory linking and memory formation can be independently regulated, and that LC to dCA1 projecting cells have a critical role in this process.

LC modulates neuronal excitability in dCA1

Memory formation is known to induce transient increases in neuronal excitability (Moyer et al., 1996; Oh and Disterhoft, 2020; Oh et al., 2010; Sehgal et al., 2014; Zhou *et al.*, 2009), thus for a time biasing the allocation of subsequent memories to the same neuronal ensembles, and consequently linking the two memories (Cai *et al.*, 2016; Rashid *et al.*, 2016; Sehgal *et al.*, 2018; Silva *et al.*, 2009; Yokose et al., 2017). Hence, LC may control contextual memory linking by modulating the persistence of dCA1 neuronal excitability.

We tested this hypothesis using the same intersectional viral strategy described above, and systemically administered CNO 30 minutes before the mice explored a novel context. The excitability of dCA1 neurons was measured 5 hours after this exposure (Fig. 3A). We found that inhibiting LC to dCA1 projecting cells reduced the firing rate of dCA1 pyramidal neurons in response to increasing steps of current injection, indicating a reduction in neuronal excitability (Fig. 3B and C). This shows that LC to dCA1 projecting cells modulate dCA1 neuronal excitability triggered by novel context exploration, a cellular mechanism previously proposed to be critical for contextual memory linking (Cai *et al.*, 2016). Furthermore, inhibition of LC neurons projecting to the dCA1 significantly increased the rheobase of dCA1 (Suppl. Table 1), which could have contributed to the reduction in firing rate. In contrast, there were no changes in the resting membrane potential (RMP), input resistance (R_{in}), peak afterhyperpolarization potential (pAHP) or action potential threshold (AP threshold) of dCA1 neurons (Suppl. Table 1). These results suggest that the inhibition of LC to dCA1 projecting cells modulates the learning-induced dCA1 neuronal intrinsic excitability, which could in turn regulate contextual memory linking.

LC modulates the overlap of contextual memory ensembles in dCA1

Recent studies have indicated that memory linking depended on the overlap between memory ensembles, since ensembles of linked memories showed more overlap than unlinked ones, and two unlinked memories could be linked simply by artificially increasing the overlap between their ensembles (Cai *et al.*, 2016; Rashid *et al.*, 2016; Yokose *et al.*, 2017). These results, together with the excitability findings presented above, suggest that LC to dCA1 projecting cells may modulate contextual memory linking by regulating the overlap between contextual memory ensembles in the dCA1.

To test this hypothesis, we injected a GCaMP6f AAV virus into dCA1 and recorded neuronal calcium ensemble activity in dCA1 with head mounted fluorescent microscopes (miniscopes) (Aharoni and Hoogland, 2019; Cai *et al.*, 2016; Ghosh *et al.*, 2011; Ziv *et al.*, 2013) while mice explored two different novel contexts (A and B) separated by 5 hours (Fig 4A). We inhibited LC neurons projecting to dCA1 while the mice explored the first context (context A), and then measured the overlap between the neuronal populations recorded during the two contextual exposures (Fig. 4A). Compared to controls, the mice with inhibition of LC neurons projecting to dCA1 showed a significant reduction in the overlap between memory ensembles activated during exploration of contexts A and B (Fig 4B). Importantly, there was no significant difference between the active population of cells detected with and without inhibition of LC neurons projecting to dCA1 (Suppl. Fig6A). Studies of c-Fos expression also confirmed that inhibition of LC neurons projecting to dCA1 did not affect the overall activation of dCA1 neurons during exploration (Suppl. Fig 6B).

Next, we tested whether the reduced overlap induced by LC-to-dCA1 inhibition was sufficient to eliminate the bias that the cells active in context B would also be allocated to the neurons previously active in context A. The results show that this probability is above chance levels in control mice, but not in mice with inhibition of LC cells projecting to dCA1 (Fig. 4C), a result consistent with our dCA1 memory ensemble overlap findings.

Furthermore, we studied the impact of this inhibition on co-activity patterns between dCA1 neurons (El-Gaby et al., 2021; Gava et al., 2021). Groups of neurons with synchronized activity have been suggested to encode task-relevant information in a number of brain structures (Buzsaki, 2010; Chang et al., 2020; Dejean et al., 2016; El-Gaby et al., 2021; Gava et al., 2021). We first defined coactivity maps for each context, as maps of pairwise temporal correlations between the activity of all dCA1 neurons that were active in both contexts (Suppl. Fig. 6G). We found that, compared to controls, inhibition of LC cells projecting to dCA1 significantly decreases the overall stability of the coactivity maps between the two contexts (Fig. 4D). To further narrow down our analysis, we identified cell assemblies (subsets of dCA1 neurons that significantly fire together) within the neurons that were active in both contexts (Lopes-dos-Santos et al., 2013). Consistently, inhibition of the LC cells projecting to dCA1 also decreased the stability of these dCA1 cell assemblies (Fig. 4E). This indicates that inhibition of LC cells projecting to dCA1 disrupts the partnerships between dCA1 neurons firing together during the exploration of context A compared to exploration of context B. Importantly, we found that the mean firing rates of the neurons that were activated in both contexts were not significantly affected (Suppl. Fig. 6C and D). This inhibition also did not affect the total number of assemblies detected (Suppl. Fig. 6E and F), or the mean pair-wise correlations (PWC) (Suppl. Fig. 6G, H and I) in either session, a result consistent with our finding that LC-dCA1 cells do not affect the formation of single contextual memories.

Together, these results strongly support the hypothesis that LC modulates contextual memory linking by biasing the co-allocation of contextual memories acquired close in time to overlapping neuronal ensembles in dCA1. Additionally, we show that LC cells projecting to dCA1 regulate the stability of assembly dynamics between the two contexts, suggesting that this is critical for linking the memories of these contexts.

Modeling the impact of LC modulation of dCA1 neuronal ensembles

Our *in vivo* experiments showed that the LC cells projecting to dCA1 were critical for the increase of neuronal excitability observed after learning. This persistent increase in excitability is thought to underlie the increased overlap between the ensembles of memories separated by hours, thereby linking those memories (Cai et al., 2016; Silva et al., 2009).

To assess whether the increase in excitability is sufficient to account for the neuronal population overlap observed in our experiments, we used a computational modeling approach. Specifically, we adapted a previously published network model (Kastellakis et al., 2016; Tzivilivaki et al., 2019), which consists of simplified spiking neurons (soma plus a few dendritic compartments) for both excitatory and inhibitory (soma-targeting and dendrite-targeting interneurons) cell types as well as calcium-dependent and protein-dependent Hebbian plasticity (Fig. 5A). In line with the experiments, we simulated the encoding of two distinct contextual memories (A and B) via the activation of two input populations that project to the excitatory model neurons (Fig 5A). Next, we simulated the LC-induced increase in excitability seen in our experiments (Fig. 3B and C) as modulation of the adaptation (AHP) current (Fig. 5B). A delay period of 5 hours was introduced between the encoding of the two memories, during which plasticity processes take place.

We simulated two conditions, control and LC-dCA1 inhibited, and analyzed the properties of the entire neuronal population after encoding the two memories. As demonstrated in the electrophysiology study, 5h after learning, the excitability of the neurons encoding context A was lower when LC neurons projecting to dCA1 were inhibited compared to the control condition. We found that simulating this difference of excitability in the network model caused a large drop in the overlap between the populations that were active (i.e. have a firing frequency > 10Hz) (Kastellakis *et al.*, 2016) during the encoding of both context A and context B (Fig. 5C), in agreement with our experimental observations. This large drop in the population overlap was not accompanied by significant changes in the sizes of the populations that were activated by either memory (Fig. 5D). These simulation results agree with our experimental observations, where inhibition of LC input to dCA1 does not affect the overall activation of dCA1 neurons during context exploration, while disrupting the overlap between two contextual memories acquired close in time.

Overall, our modeling simulations confirm that the modulation of excitability during the encoding of two separate memories, combined with Hebbian plasticity rules, can shape the overlap of populations activated by both memories without affecting their size, in agreement with our experimental hypotheses. They also indicate that mechanisms which affect the adaptation currents could be mediating the effect of the LC neuromodulatory input (Malenka and Nicoll, 1986; Pedarzani and Storm, 1995; Stanzione *et al.*, 1984).

Dopamine D1/D5 receptors in dCA1 modulate contextual memory linking

Previous studies showed that LC cells projecting to dCA1 co-release both noradrenaline and dopamine, and that these neuromodulators have differential roles in memory processes (Kempadoo *et al.*, 2016; McNamara and Dupret, 2017; Ranjbar-Slamloo and Fazlali, 2019; Takeuchi *et al.*, 2016). To determine which of these two neuromodulators mediate the effects on contextual memory linking, we implanted cannulas bilaterally into the dCA1 of mice, and treated them with either a dopamine D1/D5 receptor antagonist (SCH23390) or with a noradrenaline β -adrenergic receptor antagonist (propranolol) (Kempadoo *et al.*, 2016; Rossato *et al.*, 2009; Takeuchi *et al.*, 2016) 20 minutes before the mice explored context A. We found that the dopamine D1/D5R antagonist disrupted contextual memory linking in a dose dependent manner (Fig. 6A), while the noradrenaline β -adrenergic receptor antagonist did not (Fig. 6C). Importantly, in another set of experiments, we confirmed that the doses of the dopamine D1/D5R antagonist that disrupted contextual memory linking did not affect contextual memory itself (Fig. 6B), demonstrating that the role of dopamine in dCA1 were specific to memory linking. Together, these results indicate that dopamine (not noradrenaline) signaling in the dCA1 is critical for contextual memory linking.

Optogenetic D1 receptor activation in dCA1 rescues linking deficits caused by inhibition of LC cells projecting to dCA1

The results presented above suggested that dopaminergic modulation of the dCA1 by the LC is critical for contextual memory linking. Therefore, these results predict that the deficit in contextual memory linking, caused by inhibition of LC cells projecting to dCA1, could be rescued by activating D1 receptors in dCA1 neurons during contextual memory linking. To test this hypothesis, we used CAV-Flp in the dCA1 and Flp-dependent Gi-mCherry in the

LC (Fenno et al., 2014; Junyent and Kremer, 2015) to chemogenetically inhibit the LC cells projecting to dCA1. Simultaneously, we optogenetically activated D1 receptor signaling in a subset of dCA1 neurons expressing hSyn-cre with opto-D1 (Airan et al., 2009; Gunaydin et al., 2014) (Fig. 7A and B). We confirmed that the Flp-fDIO and cre-DIO systems were mutually exclusive: the expression of one did not affect the other (Suppl. Fig 7).

We inhibited LC cells projecting to dCA1 with CNO, administered 30 minutes before the exploration, and activated D1 receptors in dCA1 with blue light (473nm, 50s on-10s off, 10mW) while the mice explored context A, after which they were returned to their home cages. Five hours later, the mice were allowed to explore the second context (context B) without CNO infusion or blue light illumination (Fig. 7C). We confirmed that the control mice (with the DIO-GFP instead of opto-D1, in dCA1) showed a deficit in contextual memory linking, displaying freezing levels in context A that were significantly lower than in the shocked context B, and comparable to the neutral context C (Fig 7C bottom). In contrast, the mice with opto-D1 activation showed significantly higher freezing in context A compared to freezing in the neutral context C, and freezing in context A was similar to freezing in the shocked context B, demonstrating normal contextual memory linking (Fig. 7C bottom). Altogether, these results show that activation of dCA1 D1 receptors, during exploration of context A, is sufficient to rescue the loss of memory linking caused by inhibition of LC cells projecting to dCA1.

To test if opto-D1 activation rescues memory linking by restoring dCA1 excitability, we inhibited LC-dCA1 cells while activating D1R in dCA1 during context exploration as described above, and measured the excitability of dCA1 neurons after five hours. Opto-D1 activation increased the firing rate of dCA1 neurons compared to GFP controls, suggesting that the Opto-D1 receptors rescued the loss of memory linking by increasing the excitability of dCA1 neurons (Fig. 7D). Opto-D1 activation did not change the resting membrane potential (RMP), input resistance (R_{in}), rheobase, peak afterhyperpolarization potential (pAHP) or threshold to fire action potentials (AP threshold) in dCA1 neurons (Suppl. Table 2).

Together, these findings demonstrate that LC neurons projecting to dCA1 modulate contextual memory linking by regulating dCA1 excitability and the co-allocation of contextual memories to dCA1 neuronal ensembles in a dopamine-dependent manner. This discovery of a neuromodulatory system that affects memory linking without impairing memory formation, reveals a fundamental separation between the brain mechanisms that modulate these two distinct processes.

Discussion

We showed that in the absence of dopaminergic neuromodulation from LC neurons projecting to dCA1, mice exhibit normal contextual memory, but they are unable to link two contextual memories. On the other hand, the LC cells projecting to dCA3 are needed for both processes since any manipulation that impairs memory formation would also necessarily impair memory linking.

Studies have suggested that dCA1 and dCA3 are involved in different aspects of contextual/spatial memory processing (Daumas et al., 2005; Dimsdale-Zucker et al., 2018; Farovik et al., 2010; Ji and Maren, 2008). While CA1 represented objects within shared episodes as more similar than those in different episodes, CA3 differentiated the objects encountered in the same episode better (Dimsdale-Zucker *et al.*, 2018). It has been proposed that the CA3 region primarily processes information within single episodes, while the CA1 region acts primarily as a comparator that extracts and integrates information across episodes (Dimsdale-Zucker *et al.*, 2018; Molitor et al., 2021; Schapiro et al., 2017; Schlichting et al., 2014). CA1 was shown to process information about temporally ordered sequences of events with the neural code slowly changing over time, while the CA3 population activity remains highly stable (Allen et al., 2016; Davachi and DuBrow, 2015; DuBrow and Davachi, 2013; Mankin et al., 2012), allowing these two regions to manage different behavioral functions in extended time scales.

These differences between CA1 and CA3 led to the possibility that they might be differentially regulated by neuromodulation. Indeed, our results confirmed a recent study showing that the LC terminals projecting to dCA3, but not those projecting to dCA1, were necessary for single-trial contextual memory formation (Wagatsuma *et al.*, 2018).

Remarkably, we found that the LC cells projecting to dCA1 modulate the ability of one contextual memory to be linked to another acquired close in time, providing compelling evidence for a neuromodulatory pathway that regulates two distinct cognitive functions by modulating two separate subfields of the same brain structure.

Dopaminergic receptor function in dCA1 is critical for contextual memory linking

We further showed that inhibiting D1D5 receptors in dCA1 disrupts contextual memory linking, while inhibition of β -adrenergic receptors does not. Additionally, we showed that optogenetic activation of D1 signaling can rescue the LC-dependent impairment of contextual memory linking. These findings indicate that the LC modulates memory linking through dCA1 in a dopamine-dependent manner.

The focus of LC studies has been traditionally on noradrenergic function with numerous studies showing the impact of the LC-NA system in cognitive and behavioral processes, such as the regulation of waking or arousal, attention and working memory, goal-directed motivated behavior, emotional/high arousal long term memories, and fear memory retrieval (Hansen, 2017; Poe *et al.*, 2020; Ranjbar-Slamloo and Fazlali, 2019). Recently, studies have revealed a role for the dopamine co-released from the LC in memory formation (Kempadoo *et al.*, 2016; Takeuchi *et al.*, 2016; Wagatsuma *et al.*, 2018) and in long-term potentiation (Li et al., 2003), which are independent of noradrenaline, even though NA and DA receptors have been shown to interact with each other's release as well as with GABA release (Kalivas et al., 1998; Vanderschuren et al., 1999).

Additionally, the co-release of two neuromodulators from LC have been shown to have contrasting roles in social play behavior, where dopamine stimulates motivation whereas noradrenaline negatively modulates its expression (Achterberg et al., 2016). In another study

dopamine was shown to be required for a neural gain-related memory selectivity bias, while noradrenaline blockade suppressed an arousal-induced memory boost (Hauser et al., 2019).

In our work, we extend these findings beyond single memories, and show how dopamine (but not noradrenaline) during the acquisition of one memory modulates its linking to the next memory acquired within hours of the first memory. Dopamine was proposed to link novelty detection with memory destabilization to determine whether a new memory is associated with a previous reactivated engram, a result that also supports our finding that this neurotransmitter is critical for memory linking (Gonzalez *et al.*, 2021).

LC neurons projecting to dCA1 regulate memory linking by modulating neuronal excitability and the properties of memory assemblies

Our results described a neuromodulatory circuit where LC neurons projecting to dCA1 is critical in maintaining a window of increased excitability triggered by context exploration, which also leads to the allocation of memories acquired close in time to overlapping dCA1 ensembles.

LC inhibition reduced the excitability of hippocampal cells (as measured at 5h after context exploration), and this could allow formerly suppressed neighboring cells (Han et al., 2007; Rashid *et al.*, 2016) to participate in the second memory formation. Due to this competition and a winner-takes-all mechanism, upon the acquisition of the second context, the ensemble size of this context would not be reduced, and another subset of cells with similar size would encode the second memory. This was confirmed by our findings that inhibition of LC cells projecting to dCA1 does not impact the total number of dCA1 cells activated by learning. Furthermore, firing rates of principal neurons in dCA1 are known to follow a log normal-like distribution of activity with a highly active minority of neurons dominating information transmission (Mizuseki and Buzsaki, 2014). This distribution of activity was found to be difficult to disrupt by an increase in excitation (English et al., 2014), leading to an overall stability in the average firing rate (Hirase et al., 2001).

We showed that inhibition of LC cells projecting to dCA1 impairs how cells involved in one memory process subsequent information as well as the relational firing between these groups of neurons (co-activity and assemblies). Recent findings suggested that temporal correlation between neuronal activity in dCA1 encodes more information (contextual/spatial) than individual neurons, which improved behavioral performance (El-Gaby *et al.*, 2021; Gava *et al.*, 2021; Ghandour et al., 2019; Gonzalez et al., 2019), and whose stabilization depended on intrinsic excitability (Alejandre-García et al., 2020). Moreover, it was shown that dopaminergic modulation of dCA1 leads to increased neuronal coactivity and their post-learning reactivation (McNamara et al., 2014). We show that the stability of dCA1 coactivity patterns is impaired by the inhibition of LC-dCA1 cells which also disrupted memory linking.

The LC is known to modulate neuronal output in the dCA1, regulating synaptic plasticity as well as intrinsic excitability through both its dopaminergic and noradrenergic projections (Bacon et al., 2020; Olpe et al., 1986; Takeuchi *et al.*, 2016). Numerous pharmacological studies have supported the role of D₁/D₅ receptors as a gating mechanism for the persistence

of plasticity in the hippocampus (Frey et al., 1991; Huang and Kandel, 1995; Li *et al.*, 2003; Otmakhova and Lisman, 1996). For example, TH⁺ neurons in the LC were shown to boost long-lasting synaptic potentiation and memory formation through D1/D5 receptors in the CA1 (Takeuchi *et al.*, 2016). Our results demonstrate that the LC also modulates the persistence of neuronal excitability required for the neuronal overlap underlying contextual memory linking. While our convergent findings (*ex vivo*, *in vivo* and *in silico*) demonstrate a critical role for the LC-dCA1 pathway in modulating memory linking, additional pathways and circuit mechanisms may also play a role in regulating this process.

Source and relational memory problems reflect an inability to properly connect and link information about items and events acquired at different times, and they are often associated with neuropsychiatric conditions, including schizophrenia and major depression (Avery *et al.*, 2019; Jung and Lee, 2016; Nemeth *et al.*, 2016; Titone *et al.*, 2004). Thus, this study sheds light into the mechanisms underlying these deficits, and opens the door to the development of new treatments.

STAR METHODS

RESOURCE AVAILABILITY

Lead Contact—Further information and requests for resources, codes and reagents should be directed to and will be fulfilled by the Lead Contact, Alcino J Silva (silvaa@mednet.ucla.edu).

Materials availability—This study did not generate new unique reagents.

Data and code availability

- Accession numbers are listed in the key resources table. Raw data are deposited in Mendeley and are publicly available as of the date of publication. The DOI is listed in the key resources table. Microscopy and electrophysiology data reported in this paper will be shared by the lead contact upon request.
- All original code has been deposited at Zenodo and is publicly available as of the date of publication. DOIs are listed in the key resources table.
- Any additional information required to reanalyze the data reported in this paper is available from the lead contact upon request.

EXPERIMENTAL MODEL AND SUBJECT DETAILS

10–12 week-old male and female C57BL/6NTac mice were purchased from Taconic Farms (Germantown, NY) for all experiments. TH cre mice (JAX:8601, strain name: B6.Cg-Tg(TH-Cre)1Tmd/J) were purchased from Jackson laboratories and maintained in C57BL/6N background. Mice were group housed with free access to food and water, and maintained on a 12:12 hour light: dark cycle. Two weeks before an experiment, they were single-housed. All experiments were performed during the light phase of the cycle. All studies were approved by the Chancellor's Animal Research Committee at UCLA.

METHOD DETAILS

Immunostaining—Mice were transcardially perfused with 4% PFA (4% paraformaldehyde in 0.1 M phosphate buffer) and after perfusion, brains were kept in the fixation solution overnight at 4 °C, then transferred to 30% sucrose solution for 24 h, sectioned (40 µm thickness) on a cryostat and stained while free-floating.

The sections were blocked for 1 h at room temperature in 0.5% Triton-X100 in PBS (PBST) and 10% normal goat serum (Vector Laboratories, S-1000) solution. The subsequent primary and secondary antibodies were diluted in the same blocking solution. The primary antibody incubation was overnight (~24–36 h) at 4 °C, and the secondary antibody incubation was 2 h at room temperature, both with constant shaking.

Primary antibodies: chicken anti-GFP (Abcam AB13970, 1:1000), rabbit anti-cFos (Cell Signaling, 9F6, #2250, 1:500), chicken anti-TH (Abcam AB76442), guinea pig anti-RFP (SySy 390 004), rabbit anti-RFP (Rockland antibodies 600-401-379), rabbit anti-serotonin transporter antibody (Millipore Sigma, AB9726, 1:500) were used for immunostaining. Brain slices were incubated with 4',6-diaminodino-2-phenylindole (DAPI, Invitrogen, 1:1000) for 15 min, washed with PBST two times and PBS once before mounting onto slides.

Secondary antibodies were Alexa Fluor 488, 568 and 647 (Invitrogen).

Immunostaining images were acquired with a Nikon A1 Laser Scanning Confocal Microscope (LSCM) and analyzed with automatic spot-detection algorithm (Imaris 9.2, Bitplane AG).

Viral constructs—CAV2-cre and CAV2-Flp were purchased from Plateforme de Vectorologie de Montpellier, IGMM, France (Hnasko *et al.*, 2006; Soudais *et al.*, 2001).

AAV8-hSyn-DIO-hM4D(Gi)-mCherry was a gift from Bryan Roth (Addgene viral prep # 44362-AAV8; <http://n2t.net/addgene:44362> ; RRID:Addgene_44362) (Krashes *et al.*, 2011). AAV8-hSyn-DIO-mCherry was a gift from Bryan Roth (Addgene viral prep # 50459-AAV8;<http://n2t.net/addgene:50459>; RRID:Addgene_50459).

AAV1.Syn.GCaMP6f.WPRE.SV40 was a gift from Douglas Kim & GENIE Project (Addgene viral prep # 100837-AAV1; <http://n2t.net/addgene:100837>; RRID: Addgene_100837) (Chen *et al.*, 2013). AAV8-hSyn-DIO-EGFP was a gift from Bryan Roth (Addgene viral prep # 50457-AAV8; <http://n2t.net/addgene:50457>; RRID: Addgene_50457).

AAV8- Ef1a-fDIO DREADD Gi-mCherry (GVVC-AAV-171) and AAV8-Ef1a-fDIO-mCherry-WPRE (GVVC-AAV-155) were purchased from Neuroscience Gene Vector and Virus Core at Stanford, AAV1-Ef1a-fDIO EYFP was a gift from Karl Deisseroth (Addgene viral prep # 55641-AAV1; <http://n2t.net/addgene:55641> ; RRID:Addgene_55641) (Fenno *et al.*, 2014). AAV1.hSyn.Cre.WPRE.hGH was a gift from James M. Wilson (Addgene viral prep # 105553-AAV1, <http://n2t.net/addgene:105553>; RRID:Addgene_105553). AAV1.CamKII 0.4.Cre.SV40 was a gift from James M. Wilson (Addgene viral prep # 105558-AAV1; <http://n2t.net/addgene:105558>; RRID: Addgene_105558).

AAV5-EF1a-DIO-OptoD1-EYFP (UNC vector core, Chapel Hill) (Gunaydin *et al.*, 2014).

AAV-EF1a-DIO-eArch3.0-EYFP (UNC vector core, Chapel Hill)

AAV-9/2-HSYN 1-CHL-DLOX-M TAGBFP_2A_HM4D(GI)_RNRX1B(REV)-DLOX-WPRE-SV40 was purchased from University of Zurich ((Doron *et al.*, 2020; Stachniak *et al.*, 2014)

Stereotaxic Surgery—Animals were anesthetized with 3–4% isoflurane and maintained at 1.5–2% in a stereotaxic head frame on a heat pad. Artificial tears were applied to the eyes to prevent eye drying. A midline incision was made down the scalp, and a craniotomy was performed with a dental drill. After surgery, the animals were subcutaneously injected with Carprofen (5 mg/kg) and Dexamethasone (0.2 mg/kg) before recovery. Water with amoxicillin was provided for two weeks.

For virus or retrobead injection, a Nanoliter injector (World Precision Instruments) was used to infuse virus with Micro4 Controller (World Precision Instruments), injecting at coordinates relative to bregma/skull (mm): dCA1 at -1.8 (AP), ± 1.5 (ML), -1.6 (DV); dCA3 at -1.8 (AP), ± 2.0 (ML) and -2.0 (DV); LC at -5.45 (AP), ± 1.2 (ML), -3.65 (DV), RN at 4 mm (AP), -1.2 (ML at 15 degree angle), -4.5 (DV). Virus was infused at 50nL/min. After infusion, the capillary was kept at the injection site for 10 min and then withdrawn slowly. The incision was sutured and the mice were allowed to recover for 2 weeks before start of behavior.

For cannula implantation, two guide cannulas (Plastics One, C313GS-5/SPC) were implanted at the following coordinates relative to bregma (mm): AP: -2.1 , ML: ± 1.7 for dCA1. Three weeks after cannulation, mice were anesthetized and sterilized saline or drug (SCH23390, Tocris, Cat#0925; Propranolol, Tocris, Cat#0624, doses as mentioned in text, 300nl, 100nL/min) was infused into hippocampus through the internal cannula (Plastics One, C313IS-5/SPC) at DV: -1.65 relative to skull. After infusion, the internal cannula was left in place for an additional 5 min to ensure full diffusion.

For optical fiber implantation, fiber Optic Cannula (Newdoon, 200 μm , NA=0.37) was immediately implanted after virus injection. The tip of the optic fiber was placed 1mm above the virus injection site. Then, the canula was fixed with Metabond and dental cement.

For miniscope implantation, a GRIN lens was implanted into the dorsal hippocampal CA1 region as previously described (Cai *et al.*, 2016). After GCaMP6f virus injection, a $\sim 2\text{mm}$ diameter circular craniotomy was centered at the injection site. The cortex directly below the craniotomy was aspirated with a 27-gauge blunt syringe needle attached to a vacuum pump. Cortex buffer (NaCl 135mM, KCL 5mM, CaCl₂ 2.5mM, MgSO₄ 1.3mM, HEPES 5mM, PH 7.4) was repeatedly applied to the exposed tissue to prevent drying. The GRIN lens (0.52 NA, 1.8 mm in diameter, Edmund Optics) was slowly lowered above CA1 to a depth of 1.35 mm ventral to the surface of the skull at the most posterior point of the craniotomy. Next, a skull screw was used to anchor the lens to the skull. Both the lens and skull screw were fixed with super glue (Loctite, 45198) and dental cement (Jet Denture Repair Package, Lang, 1223CLR). Low Toxicity Silicone Adhesive (Kwik-Sil, World Precision Instruments)

was used to cover the GRIN Lens for protection. Two weeks later, a small baseplate was cemented onto the animal's head atop the previously formed dental cement.

Behavioral procedures—Two weeks after surgeries, the mice were first handled for 5 days (2min/day) in their housing room, and then habituated to transportation and external environmental cues for 2 minutes in the experimental room each day where they were also handled (2min/day) for another 3 days. In the contextual memory linking task, mice explored 2 different contexts (A and then B) which were separated by 5 hours. Mice explored each context for 10 min. CNO injection (Tocris, Cat#4936, 5mg/kg, i.p) or drug infusions were done as noted. For immediate shock, two days later, mice were placed in chamber B for 10 s followed by a 2s shock (0.75 mA). 58 seconds after the shock, mice were placed back in their home cage. For the context tests, mice were returned to the designated context for the next three days (A, B and a new neutral context C) in a counterbalanced manner. Contexts A and C were counterbalanced. Freezing was assessed via an automated scoring system (Med Associates) with 30 frames per second sampling; the mice needed to freeze continuously for at least one second before freezing could be counted.

For the analysis for movement with or without CNO, we tracked the position of the animals in the open field using idTracker, an open-source tracking algorithm (Perez-Escudero et al., 2014), which outputs frame-wise XY coordinates of the position of the animal in pixels. The distance traveled was calculated as the sum of the magnitudes of the displacement vectors between the positions of the animal in subsequent frames. The distance traveled was converted from pixels into centimeters by using a reference with known length within the camera field of view but outside the open field. The Average Speed was calculated as the ratio between the distance traveled and the total duration of the session in seconds.

For single contextual memory, the mice were handled and habituated the same way. They explored one context for 10min, and two days later, the mice were placed in that chamber for 10 s followed by a 2s shock (0.75 mA). 58 seconds after the shock, mice were placed back in their home cages. For the context tests, mice were returned to the shocked context and a counterbalanced neutral context.

Optogenetics—Two weeks after virus injection and optic cannula implantation, the mice were handled for 5 days (2min/day) in their housing room, and then handled in their experimental room for another 5 days where they were additionally habituated with the optic fiber connected in their home cage (2min/day). On the day of behavioral linking, they were systemically (i.p) injected with CNO (5mg/kg) 30min before context A where they received light stimulation during the 10 min exploration (Blue: 473nm, 8–10mW, 50s on/10s off; Green: 566 nm, 15–20 mW, for OptoD1 and Arch respectively). Five hours later, they were taken to explore context B for 10min without drug or optic fiber.

Computational modeling—A previously published model network of memory allocation was adapted (Kastellakis *et al.*, 2016). The model network consists of populations of excitatory and inhibitory neurons which are modeled as 2-stage integrators to account for dendrites. Neurons consist of a somatic unit connected to independent dendritic subunits. Both dendrites and soma are modeled using simplified integrate-and-fire model dynamics,

where the somatic unit includes adaptation current, while dendritic units receive excitatory synaptic currents. Dendrites and soma are coupled via axial resistance. Inhibitory neurons provide feedback inhibition and are separated in 2 equal sub-populations, soma-targeting and dendrite-targeting. Each dendritic subunit integrates incoming the synaptic inputs which reside on it independently as follows:

$$C \frac{dV_d}{dt} = g_E(E_E - V_d) - g_I(E_I - V_d) - g_L(V_d - E_L)$$

Where V_d is the dendritic depolarization, C is the membrane capacitance of, E_E is the reversal potential for excitatory receptors, E_I is the reversal potential for inhibitory receptors, E_L is the resting potential (0mV), g_L is the leak conductance and g_E, g_I are the instantaneous activations of synaptic currents

$$g_{E/I}(t) = \sum_{i,j} w_j \delta(t - t_{i,j})$$

Where w_j is the weight of synapse j and $t_{i,j}$ are the timings of incoming spikes.

Somatic spiking follows an Integrate and Fire model with adaptation:

$$C \frac{dV}{dt} = -g_L(V - E_L) + I_{noise}(t) + I_{ax}(t) - I_{inh}(t) - I_{adapt}(t)$$

$$\tau_{adapt} \frac{dI_{adapt}}{dt} = \alpha_{adapt} * (V - E_L) + \beta_{adapt} \delta(t - t_{spike}) - I_{adapt}$$

$$I_{ax} = \sum_n g_{ax}(V_{d,i} - V)_+$$

$$\tau_{inh} \frac{dI_{inh}}{dt} = \sum_i g_{inh} \delta(t - t_i) - I_{inh}$$

Where V is the somatic voltage, I_{noise} is uniform noise current (max amplitude 500 pA), I_{ax} is the excitatory axial current, I_{inh} is the filtered inhibitory input from somatically-targeting interneurons, I_{adapt} is the adaptation current, τ_{adapt} is the adaptation time constant, α_{adapt} the adaptation coupling parameter, β_{adapt} is the amount by which adaptation current increases every time the neuron spikes, g_{ax} is the axial resistance, τ_{inh} is the time constant of inhibitory current and g_{inh} the inhibitory current scaling constant.

Somatic spiking occurs when the somatic voltage reaches the spike threshold θ_{soma} . Calcium influx is recorded on the level of single synapses, branches and whole neuron. Synaptic and dendritic branch calcium is increased when a presynaptic spike coincides with back propagating action potential. Somatic calcium is increased by every time a somatic spike

occurs. For plasticity-induction purposes the overall sum of accumulated calcium at the end of a 4 second stimulation is used.

Synapses representing memories to be encoded are initially allocated randomly to the dendritic subunits of pyramidal neurons with initial weight 0.4. In addition, feedback synapses between pyramidal and inhibitory populations are allocated at random, with separate distributions for soma-targeting and dendrite-targeting interneurons.

Calcium influx in a synapse during a 4 second stimulus presentation determines plasticity, which is dependent on the availability of plasticity-related proteins (PRPs). Synapses are selected for plasticity according to a Hebbian rule: Synapses that receive significant calcium influx and reside on a neuron that is highly activated are selected for potentiation, otherwise they are selected for depression. The update of the weights of the selected is dependent on the level of Plasticity-Related-Protein (PRP) synthesis, which is assumed to be somatic. The level of PRPs after the somatic calcium level exceeds the threshold Θ_{PRP} over time in minutes follows the alpha function

$$PRP(t) = (t - 20min)e^{1 - \frac{t - 20min}{30 min}}$$

The sum of available proteins determines the rate of consolidation of the weights w of synapses. Synaptic weights are also subject to a homeostatic plasticity rule, which normalizes the total synaptic input to each neuron over long time scales:

$$\frac{dw_j}{dt} = \frac{1}{\tau_H} \left(1 - \frac{\sum_j w_j}{w_{init} N_{syn}} \right)$$

Where w_{init} is the 0.3, N_{syn} the total number of synapses in the neuron and τ_H the time constant of homeostatic synaptic scaling.

Simulation of memory formation takes place according to the following protocol: For every memory being encoded, the inputs which represent the memory are stimulated for 4 seconds with a high firing rate (80Hz) to drive the firing of the initially-weak synapses. After the first memory encoding, protein dynamics and excitability modulation are modeled for 5 hours as detailed in (Kastellakis *et al.*, 2016) and then the second memory is encoded. The neurons which have firing rate >10Hz during encoding are considered as highly-active and thus part of the memory engrams. Under control conditions, the excitability of these neurons is increased after encoding for a period of up to 12 hours. Under the LC block condition, this increase in excitability does not take place. The overlap between active populations is measured by the ratio of (neurons active in both memories) / (neurons active in either memory). For additional details of the model see (Kastellakis *et al.*, 2016). The parameters used are listed in Supplementary Table 2. The model was written in C++. The source code for the simulation, data analysis and scripts to reproduce the data and figures are available in the ModelDB database (Accession Number 267173).

Slice Preparation

Inhibition of LC-dCA1 projecting cells (Fig. 3): Adult mice injected with a CAV-Cre virus in the dCA1 and either AAV-hSyn-DIO-hM4D(Gi)-mCherry or AAV-hSyn-DIO-mCherry in the LC and were administered clozapine-N-oxide (CNO, 5mg/kg, i.p) 30 min prior to context exploration. The mice were allowed to explore a novel context for 10 min and five hours later were deeply anaesthetized with isoflurane and decapitated.

Opto-D1 rescue of excitability (Fig. 7D): Adult mice were injected with a CAV-Flp virus in the dCA1, a Flp-dependent (Frt) AAV-fDIO-hM4i-DREADD-mCherry in the LC and a cocktail of either AAV-hSyn-cre and AAV-DIO-optoD1-GFP or AAV-hSyn-cre and AAV-DIO-GFP in the dCA1. An optical fiber was implanted 1mm above the dCA1 injection site. The mice were habituated to the connected optic fiber as described above. On the day of behavioral linking, they were systemically (i.p) injected with CNO (5mg/kg) 30min before a 10 min context exploration where they received light stimulation (473nm, 8–10mW, 50s on/10s off). Five hours later, the mice were deeply anaesthetized with isoflurane and decapitated.

Inhibition of LC neurons with hM4Di (Suppl. Fig. 2): Adult mice injected with a CAV-Cre virus in the dCA1 and AAV-hSyn-DIO-hM4D(Gi)-mCherry in the LC.

The brain was rapidly dissected out and transferred to oxygenated (95% O₂ / 5% CO₂), ice-cold cutting solution containing (in mM): 93 NMDG, 93 HCl, 2.5 KCl, 1.2 NaH₂PO₄, 30 NaHCO₃, 20 HEPES, 25 glucose, 2 Thiourea, 5 Na-ascorbate, 3 Na-pyruvate, 5 N-acetyl-L-cysteine, 2 CaCl₂ and 2 MgCl₂. Coronal slices (300 μm thick) containing the hippocampus were cut using a Leica VT1200 vibrating blade microtome, transferred to a submerged holding chamber containing oxygenated cutting solution and allowed to recover for 15 min at 34°C. Following recovery, the slices were transferred to an oxygenated solution containing (in mM): 92 HEPES, 2.5 KCl, 1.2 NaH₂PO₄, 30 NaHCO₃, 20 HEPES, 25 glucose, 2 Thiourea, 5 Na-ascorbate, 3 Na-pyruvate, 5 N-acetyl-L-cysteine, 2 CaCl₂ and 2 MgCl₂ and allowed to recover further for 1hr. Following incubation, slices were transferred to a superfused recording chamber and constantly perfused with oxygenated aCSF containing (in mM): 115 NaCl, 10 glucose, 25.5 NaHCO₃, 1.05 NaH₂PO₄, 3.3 KCl, 2 CaCl₂ and 1 MgCl₂ and maintained at 28°C.

Whole-cell patch recordings—Whole cell current-clamp recordings were performed on pyramidal neurons in the dorsal CA1 region of the hippocampus (Fig. 3 and Fig. 7D) and on mCherry⁺ excitatory neurons in the LC (Suppl. Fig. 2) using pipettes (3–5MΩ resistance) pulled from thin-walled Borosilicate glass using a Sutter P97 Flaming/Brown micropipette puller and filled with an internal solution containing (in mM) 120 K-methylsulfate, 10 KCl, 10 HEPES, 10 Na-phosphocreatine, 4 Mg-ATP and 0.4 Na-GTP. All recordings were obtained using a MultiClamp 700B amplifier controlled by the pClamp 10 software and digitized using the Digidata 1440A system. Signals were filtered at 10kHz and digitized at 20kHz. Neurons were included in the study only if the initial resting membrane potential (V_m) –55 mV, access resistance (R_a) was <25MΩ and were rejected if the R_a changed by >20% of its initial value. For all recordings, dCA1 neurons were held at –65 mV and

LC neurons were held at -60 mV. The stable resting membrane potential of neurons were measured and averaged over a 60s duration with 0mA current injection immediately after breaking in. Input resistance was measured as the slope of the steady-state voltage response to increasing current injections (-50 pA to 50 pA, $\Delta = 10$ pA). To investigate the firing rate of neurons, the number of action potentials fired in response to a 600 ms pulse of depolarizing current injection (0 pA to 480 pA in 20 pA increments) was calculated. Three pulses were delivered for each current amplitude and the average number of action potentials fired for each current amplitude was plotted. Rheobase was measured as the minimum current injection required to elicit an action potential. The amplitude of peak afterhyperpolarization potentials (pAHP) were measured as the maximum hyperpolarization immediately following a burst of action potentials. The threshold voltage to fire an action potential (AP threshold) was calculated across 10 sweeps of 600 ms current pulse where the neuron fired 2–4 action potentials. To study the inhibitory effect of hM4Di on neurons (Suppl. Fig. 3), the firing rate of LC neurons was measured as described above during baseline and in the presence of 10μ M CNO. The recordings were analyzed using Stimfit 0.15.8 (Guzman et al., 2014)

Miniscope analysis—One-photon calcium imaging was recorded using UCLA miniscopes (Aharoni et al., 2019; Cai *et al.*, 2016). During recordings, digital imaging data were sent from the CMOS imaging sensor (Aptina, MT9V032) to custom data acquisition (DAQ) electronics and USB Host Controller (Cypress, CYUSB3013) over a light weight, highly flexible co-axial cable. Images were acquired at 30 frames per second, using display resolution at 752×480 pixels (1 pixel = $1-2\mu$ m), and saved into uncompressed avi files. The analysis pipeline was written in MATLAB using first the NoRMCorre algorithm for motion correction (rigid registration) (Pnevmatikakis and Giovannucci, 2017), followed by individual neuron identification and extraction using the CNMF-E algorithm (Zhou et al., 2018). During motion correction, videos were 2x spatially downsampled using the default built-in NoRMCorre protocol. During CNMF-E initialization, videos were further 2x spatially down-sampled and 5x temporally down-sampled. After motion correction, the videos were analyzed in two different ways. In the single session analysis, videos from individual sessions were directly input for CNMF-E processing; while in the concatenated analysis, these videos were first aligned and then concatenated before CNMF-E analysis (Concat Pipeline). Alignment was performed using a semi-automatic alignment tool based on the “imregtform” function (Matlab – image processing toolbox) followed by manual checking of landmarks (usually blood vessels).

After concatenation and CNMF-E processing, the quality of neuron extraction in the concatenated analysis was verified using a MATLAB custom-made Neuron Deletion GUI. Putative false-positive neurons were filtered out using the following exclusion criteria: 1) abnormalities on ROI morphology or calcium trace, and 2) calcium trace peaks with no corresponding fluorescence increases in the video. Experimenters were blinded to all steps of the analysis. All downstream analysis was performed using the remaining ROIs after filtering (putative neurons). Neurons detected on the CNMF-E analysis on single 10-min sessions were only used if they found a correspondent match on the filtered concatenated analysis. We used the spatial foot prints (neuron.A, output from CNMF-E) from each one of the detected cells for the binary matching analysis between each one of the single

sessions and the filtered concatenated analysis. The centroid distance and spatial correlation were calculated for all cell pairs (concatenated x single session). Cells were deemed as a match if their spatial correlation ≥ 0.8 and their centroid distance ≤ 5 pixels. We defined the percentage overlap between 2 given sessions (e.g., A and B) as the ratio between the intersection ($A \cap B$) and the union ($A \cup B$) among the cells activated in the respective sessions, as in the formula:

$$\text{Overlap}(\%)_{AB} = \frac{\text{Cells active in A and B}}{\text{Cells active in A or B}} \times 100$$

The probabilistic calculations on activated cells were defined as the conditional probability of cells to have been retrospectively active during LC manipulation 5h in the past, given that they are active during exploration of the following context. This indicates the likelihood that the cells activated during exploration of a novel context were biased by the cells activated during exploration of another novel context 5h before, and is formally calculated as:

$$P(A | B) = \frac{P(A \cap B)}{P(B)},$$

where $P(A \cap B)$ and $P(B)$ are respectively the probability of cells being active in A and B and the probability of cells being active in B. These probabilities were defined as the ratios $P(A \cap B) = \text{Cells active in A and B}/U$ and $P(B) = \text{Cells active in B}/U$, in which U was defined as the universe (total number) of cells detected in the concatenated analysis.

For the analysis of neuronal activity dynamics across sessions, the raw calcium traces (neuron.C_raw) extracted from putative neurons using CNMF-E were deconvolved into spike probabilities using the foopsi thresholded method (OASIS toolbox) (Friedrich et al., 2017). Finally, the spike probabilities from single frames were binarized between 1 (active) and 0 (inactive). Mean firing rate was calculated as the number of active frames per second within the overlapping neuronal population in each context. The coactivity map from a specific session was defined as the matrix containing all the pairwise temporal correlations (PWC, Pearson Correlation) between the binned activity (100 ms) of any two given neurons. Mean PWC was calculated as the average of all values within a coactivity map of overlapping neurons, discarding autocorrelations (correlation between a given neuron and itself).

PWC stability represents the stability of how neurons fire together across both contexts. PWC stability is calculated by converting the coactivity values for all overlapping neurons with themselves in each session into a vector, and then measuring the Pearson linear correlation between these vectors. To avoid potential high-correlation false positives due to fluorescence leak through between putative neurons that are spatially close to each other, we excluded the correlation-pairs between neurons that had overlapping spatial footprints or had centroids closer than 20 pixels from one another. PWC stability values closer to 1 means that neurons tend to keep their partnership profile (fire together, show independent activity, or fire when the other remains silent) in both contexts. Representative graphs to visualize the PWC stability (Fig. 4E) were generated by calculating the absolute delta between the

PWC matrices in context B vs context A. To prevent ensemble size effects, PWC stability was calculated in subsamples of the neurons from individual animals (1000 permutations), equal to the smallest number of overlapping neurons detected in all animals. The final PWC stability value for each animal was defined as the average of these 1000 values.

Cell assemblies within the overlapping neuron population were identified using a PCA/ICA mathematical tool based on Hebbian co-firing rules (Lopes-dos-Santos *et al.*, 2013). This method identifies a number of co-activation patterns for every dataset (in the case of our dataset, between 1–6 patterns per session for the overlapping neuron population) characterized by a linear correlation between the activity of the cells within each assembly. For each assembly detected, every recorded cell will have a weight representing how much that cell fires together with other cells that participate in the assembly. This weight score can go from +1 to -1, corresponding to a range of perfect correlation to perfect anti-correlation between the firing of that specific neuron and the activity of the assembly pattern. A high absolute weight means the neuron is a part of that assembly, while a low absolute weight means it is not a part of the assembly.

The cell assembly detection framework can be summarized by these three main steps:

1. **Generation of the Activity Matrix:** the neuronal activity was binned (100ms) and normalized by z-score (variance is set to 1 and mean is set to 0).
2. **Detection of Cell Assemblies:** PCA was performed in the Activity Matrix to identify its principal components (putative assemblies). Parallel to that, a random circular shift method was used on each neuronal activity independently, breaking any real temporal correlation between neurons. The shifted neuronal activity was used to estimate surrogate Activity Matrices and their respective eigenvalues (200 permutations), which were used to define a random distribution. Principal components of the original Activity Matrix with associated eigenvalues statistically different (95% threshold) from the randomized distribution were considered significant cell assemblies.
3. **Generation of Assembly Patterns:** Independent Components Analysis (ICA) was performed on the original Activity Matrix projected on the subspace spanned by the patterns of the significant cell assemblies. The output independent components can be understood as assembly patterns in which values attributed to each neuron define the weights of the cells (relative relevance) in the corresponding assembly.

Stability Index (SI) for cell assemblies represents how similar the weights for matching assemblies are maintained across the two contexts. First, a similarity index was calculated by measuring the cosine similarity (inner product) between all identified cell assembly patterns in the overlapping neuron population of context B (second exposure) versus context A (first exposure) (Almeida-Filho *et al.*, 2014). Assemblies of context B were then matched in a 1:1 ratio to the assembly from context A with the highest similarity value. Stability index was then calculated by averaging the similarity values of all matched assemblies.

QUANTIFICATION AND STATISTICAL ANALYSIS

The investigators who collected and analyzed the data including behavior, electrophysiological and staining were blinded to the experimental conditions. Error bars in the figures indicate the SEM. Sample sizes were chosen on the basis of previous studies from the lab. All statistical analyses were performed using GraphPad Prism 9.0.2 (GraphPad Software, La Jolla, California USA). For behavior and immunohistochemistry experiments, *n* designates the number of mouse. For electrophysiological measurements, *n* designates the number of neurons. Statistical significance was assessed by unpaired- *t* test (two-tailed), Mann-Whitney, one-sample *t*-test, one-way ANOVA, two-way RM ANOVA where appropriate, followed by the indicated post-hoc tests. Normality was tested by Shapiro-Wilk and Kolmogorov-Smirnov tests. The level of significance was set at $p < 0.05$. Data points deviating more than 2 SD values from the mean were excluded from the analyses.

Supplementary Material

Refer to Web version on PubMed Central for supplementary material.

Acknowledgements:

We thank Yang Shen, Megha Sehgal, Ying Cai and Andre Sousa for technical support and advice, and Dietmar Schmitz for supporting AT's work. This study was supported by grants from the NIMH (R01 MH113071), NIA (R01 AG013622), NINDS (R01 NS106969), from the Dr. Miriam and Sheldon G. Adelson Medical Research Foundation to A.J.S, the SNSF postdoc fellowship to AC, PEW fellowship to DAF. AT was supported by Einstein Center for Neurosciences Ph.D. Fellowship, SFB1315. The computational modelling work was supported by the European Commission (H2020-FETOPEN-2018-2019-2020-01, FET-Open project NEUREKA, GA-863245), the NIH (R01MH124867-01) and the Einstein Foundation Berlin (EVF-2019-508).

Inclusion and Diversity statement:

We worked to ensure sex balance in the selection of non-human subjects. One or more of the authors of this paper self-identifies as an underrepresented ethnic minority in science. One or more of the authors of this paper self-identifies as living with a disability. One or more of the authors of this paper received support from a program designed to increase minority representation in science. While citing references scientifically relevant for this work, we also actively worked to promote gender balance in our reference list.

References:

- Achterberg EJ, van Kerkhof LW, Servadio M, van Swieten MM, Houwing DJ, Aalderink M, Driel NV, Trezza V, and Vanderschuren LJ (2016). Contrasting Roles of Dopamine and Noradrenaline in the Motivational Properties of Social Play Behavior in Rats. *Neuropsychopharmacology* 41, 858–868. 10.1038/npp.2015.212. [PubMed: 26174597]
- Aharoni D, and Hoogland TM (2019). Circuit Investigations With Open-Source Miniaturized Microscopes: Past, Present and Future. *Frontiers in cellular neuroscience* 13, 141. 10.3389/fncel.2019.00141. [PubMed: 31024265]
- Aharoni D, Khakh BS, Silva AJ, and Golshani P (2019). All the light that we can see: a new era in miniaturized microscopy. *Nat Methods* 16, 11–13. 10.1038/s41592-018-0266-x. [PubMed: 30573833]

- Airan RD, Thompson KR, Fenno LE, Bernstein H, and Deisseroth K (2009). Temporally precise in vivo control of intracellular signalling. *Nature* 458, 1025–1029. 10.1038/nature07926. [PubMed: 19295515]
- Alejandre-García T, Kim S, Pérez-Ortega J, and Yuste R (2020). Intrinsic excitability mechanisms of neuronal ensemble formation. *bioRxiv*, 2020.2007.2029.223966. 10.1101/2020.07.29.223966.
- Allen TA, Salz DM, McKenzie S, and Fortin NJ (2016). Nonspatial Sequence Coding in CA1 Neurons. *The Journal of neuroscience : the official journal of the Society for Neuroscience* 36, 1547–1563. 10.1523/JNEUROSCI.2874-15.2016. [PubMed: 26843637]
- Almeida-Filho DG, Lopes-dos-Santos V, Vasconcelos NA, Miranda JG, Tort AB, and Ribeiro S (2014). An investigation of Hebbian phase sequences as assembly graphs. *Front Neural Circuits* 8, 34. 10.3389/fncir.2014.00034. [PubMed: 24782715]
- Armbruster BN, Li X, Pausch MH, Herlitze S, and Roth BL (2007). Evolving the lock to fit the key to create a family of G protein-coupled receptors potently activated by an inert ligand. *Proc Natl Acad Sci U S A* 104, 5163–5168. 10.1073/pnas.0700293104. [PubMed: 17360345]
- Avery MC, and Krichmar JL (2017). Neuromodulatory Systems and Their Interactions: A Review of Models, Theories, and Experiments. *Front Neural Circuits* 11, 108. 10.3389/fncir.2017.00108. [PubMed: 29311844]
- Avery SN, Armstrong K, Blackford JU, Woodward ND, Cohen N, and Heckers S (2019). Impaired relational memory in the early stage of psychosis. *Schizophr Res* 212, 113–120. 10.1016/j.schres.2019.07.060. [PubMed: 31402078]
- Bacon TJ, Pickering AE, and Mellor JR (2020). Noradrenaline Release from Locus Coeruleus Terminals in the Hippocampus Enhances Excitation-Spike Coupling in CA1 Pyramidal Neurons Via beta-Adrenoceptors. *Cereb Cortex* 30, 6135–6151. 10.1093/cercor/bhaa159. [PubMed: 32607551]
- Buzsáki G (2010). Neural syntax: cell assemblies, synapse ensembles, and readers. *Neuron* 68, 362–385. 10.1016/j.neuron.2010.09.023. [PubMed: 21040841]
- Cai DJ, Aharoni D, Shuman T, Shobe J, Biane J, Song W, Wei B, Veshkini M, La-Vu M, Lou J, et al. (2016). A shared neural ensemble links distinct contextual memories encoded close in time. *Nature* 534, 115–118. 10.1038/nature17955. [PubMed: 27251287]
- Chang H, Esteves IM, Neumann AR, Sun J, Mohajerani MH, and McNaughton BL (2020). Coordinated activities of retrosplenial ensembles during resting-state encode spatial landmarks. *Philos Trans R Soc Lond B Biol Sci* 375, 20190228. 10.1098/rstb.2019.0228.
- Chen TW, Wardill TJ, Sun Y, Pulver SR, Renninger SL, Baohan A, Schreiter ER, Kerr RA, Orger MB, Jayaraman V, et al. (2013). Ultrasensitive fluorescent proteins for imaging neuronal activity. *Nature* 499, 295–300. 10.1038/nature12354. [PubMed: 23868258]
- Chowdhury A, and Caroni P (2018). Time units for learning involving maintenance of system-wide cFos expression in neuronal assemblies. *Nat Commun* 9, 4122. 10.1038/s41467-018-06516-3. [PubMed: 30297716]
- Cohen JY, Amoroso MW, and Uchida N (2015). Serotonergic neurons signal reward and punishment on multiple timescales. *eLife* 4. 10.7554/eLife.06346.
- Daumas S, Halley H, Frances B, and Lassalle JM (2005). Encoding, consolidation, and retrieval of contextual memory: differential involvement of dorsal CA3 and CA1 hippocampal subregions. *Learn Mem* 12, 375–382. 10.1101/lm.81905. [PubMed: 16027176]
- Davachi L, and DuBrow S (2015). How the hippocampus preserves order: the role of prediction and context. *Trends in cognitive sciences* 19, 92–99. 10.1016/j.tics.2014.12.004. [PubMed: 25600586]
- de Sousa AF, Chowdhury A, and Silva AJ (2021). Dimensions and mechanisms of memory organization. *Neuron*. 10.1016/j.neuron.2021.06.014.
- Dejean C, Courtin J, Karalis N, Chaudun F, Wurtz H, Bienvenu TC, and Herry C (2016). Prefrontal neuronal assemblies temporally control fear behaviour. *Nature* 535, 420–424. 10.1038/nature18630. [PubMed: 27409809]
- Dimsdale-Zucker HR, Ritchey M, Ekstrom AD, Yonelinas AP, and Ranganath C (2018). CA1 and CA3 differentially support spontaneous retrieval of episodic contexts within human hippocampal subfields. *Nat Commun* 9, 294. 10.1038/s41467-017-02752-1. [PubMed: 29348512]

- Doron G, Shin JN, Takahashi N, Druke M, Bocklisch C, Skenderi S, de Mont L, Toumazou M, Ledderose J, Brecht M, et al. (2020). Perirhinal input to neocortical layer 1 controls learning. *Science* 370. 10.1126/science.aaz3136.
- DuBrow S, and Davachi L (2013). The influence of context boundaries on memory for the sequential order of events. *J Exp Psychol Gen* 142, 1277–1286. 10.1037/a0034024. [PubMed: 23957281]
- Duszkiewicz AJ, McNamara CG, Takeuchi T, and Genzel L (2019). Novelty and Dopaminergic Modulation of Memory Persistence: A Tale of Two Systems. *Trends Neurosci* 42, 102–114. 10.1016/j.tins.2018.10.002. [PubMed: 30455050]
- El-Gaby M, Reeve HM, Lopes-Dos-Santos V, Campo-Urriza N, Perestenko PV, Morley A, Strickland LAM, Lukacs IP, Paulsen O, and Dupret D (2021). An emergent neural coactivity code for dynamic memory. *Nature neuroscience* 24, 694–704. 10.1038/s41593-021-00820-w. [PubMed: 33782620]
- English DF, Peyrache A, Stark E, Roux L, Vallentin D, Long MA, and Buzsaki G (2014). Excitation and inhibition compete to control spiking during hippocampal ripples: intracellular study in behaving mice. *The Journal of neuroscience : the official journal of the Society for Neuroscience* 34, 16509–16517. 10.1523/JNEUROSCI.2600-14.2014.
- Farovik A, Dupont LM, and Eichenbaum H (2010). Distinct roles for dorsal CA3 and CA1 in memory for sequential nonspatial events. *Learn Mem* 17, 12–17. 10.1101/lm.1616209. [PubMed: 20028733]
- Fenno LE, Mattis J, Ramakrishnan C, Hyun M, Lee SY, He M, Tucciarone J, Selimbeyoglu A, Berndt A, Grosenick L, et al. (2014). Targeting cells with single vectors using multiple-feature Boolean logic. *Nature methods* 11, 763–772. 10.1038/nmeth.2996. [PubMed: 24908100]
- Frey U, Matthies H, Reymann KG, and Matthies H (1991). The effect of dopaminergic D1 receptor blockade during tetanization on the expression of long-term potentiation in the rat CA1 region in vitro. *Neurosci Lett* 129, 111–114. 10.1016/0304-3940(91)90732-9. [PubMed: 1833673]
- Friedrich J, Zhou P, and Paninski L (2017). Fast online deconvolution of calcium imaging data. *PLoS computational biology* 13, e1005423. 10.1371/journal.pcbi.1005423.
- Gava GP, McHugh SB, Lefevre L, Lopes-Dos-Santos V, Trouche S, El-Gaby M, Schultz SR, and Dupret D (2021). Integrating new memories into the hippocampal network activity space. *Nature neuroscience* 24, 326–330. 10.1038/s41593-021-00804-w. [PubMed: 33603228]
- Ghandour K, Ohkawa N, Fung CCA, Asai H, Saitoh Y, Takekawa T, Okubo-Suzuki R, Soya S, Nishizono H, Matsuo M, et al. (2019). Orchestrated ensemble activities constitute a hippocampal memory engram. *Nat Commun* 10, 2637. 10.1038/s41467-019-10683-2. [PubMed: 31201332]
- Ghosh KK, Burns LD, Cocker ED, Nimmerjahn A, Ziv Y, Gamal AE, and Schnitzer MJ (2011). Miniaturized integration of a fluorescence microscope. *Nature methods* 8, 871–878. 10.1038/nmeth.1694. [PubMed: 21909102]
- Gonzalez MC, Rossato JI, Radiske A, Bevilaqua LRM, and Cammarota M (2021). Dopamine controls whether new declarative information updates reactivated memories through reconsolidation. *Proc Natl Acad Sci U S A* 118. 10.1073/pnas.2025275118.
- Gonzalez WG, Zhang H, Harutyunyan A, and Lois C (2019). Persistence of neuronal representations through time and damage in the hippocampus. *Science* 365, 821–825. 10.1126/science.aav9199. [PubMed: 31439798]
- Gunaydin LA, Grosenick L, Finkelstein JC, Kauvar IV, Fenno LE, Adhikari A, Lammel S, Mirzabekov JJ, Airan RD, Zalocusky KA, et al. (2014). Natural neural projection dynamics underlying social behavior. *Cell* 157, 1535–1551. 10.1016/j.cell.2014.05.017. [PubMed: 24949967]
- Guzman SJ, Schlogl A, and Schmidt-Hieber C (2014). Stimfit: quantifying electrophysiological data with Python. *Front Neuroinform* 8, 16. 10.3389/fninf.2014.00016. [PubMed: 24600389]
- Han JH, Kushner SA, Yiu AP, Cole CJ, Matynia A, Brown RA, Neve RL, Guzowski JF, Silva AJ, and Josselyn SA (2007). Neuronal competition and selection during memory formation. *Science* 316, 457–460. 10.1126/science.1139438. [PubMed: 17446403]
- Han JH, Kushner SA, Yiu AP, Hsiang HL, Buch T, Waisman A, Bontempi B, Neve RL, Frankland PW, and Josselyn SA (2009). Selective erasure of a fear memory. *Science* 323, 1492–1496. 10.1126/science.1164139. [PubMed: 19286560]

- Hansen N (2017). The Longevity of Hippocampus-Dependent Memory Is Orchestrated by the Locus Coeruleus-Noradrenergic System. *Neural Plast* 2017, 2727602. 10.1155/2017/2727602.
- Hauser TU, Eldar E, Purg N, Moutoussis M, and Dolan RJ (2019). Distinct Roles of Dopamine and Noradrenaline in Incidental Memory. *The Journal of neuroscience : the official journal of the Society for Neuroscience* 39, 7715–7721. 10.1523/JNEUROSCI.0401-19.2019. [PubMed: 31405924]
- Hirase H, Leinekugel X, Czurko A, Csicsvari J, and Buzsaki G (2001). Firing rates of hippocampal neurons are preserved during subsequent sleep episodes and modified by novel awake experience. *Proc Natl Acad Sci U S A* 98, 9386–9390. 10.1073/pnas.161274398. [PubMed: 11470910]
- Hnasko TS, Perez FA, Scouras AD, Stoll EA, Gale SD, Luquet S, Phillips PE, Kremer EJ, and Palmiter RD (2006). Cre recombinase-mediated restoration of nigrostriatal dopamine in dopamine-deficient mice reverses hypophagia and bradykinesia. *Proc Natl Acad Sci U S A* 103, 8858–8863. 10.1073/pnas.0603081103. [PubMed: 16723393]
- Huang YY, and Kandel ER (1995). D1/D5 receptor agonists induce a protein synthesis-dependent late potentiation in the CA1 region of the hippocampus. *Proc Natl Acad Sci U S A* 92, 2446–2450. 10.1073/pnas.92.7.2446. [PubMed: 7708662]
- Ji J, and Maren S (2008). Differential roles for hippocampal areas CA1 and CA3 in the contextual encoding and retrieval of extinguished fear. *Learn Mem* 15, 244–251. 10.1101/lm.794808. [PubMed: 18391185]
- Jung W, and Lee SH (2016). Memory deficit in patients with schizophrenia and posttraumatic stress disorder: relational vs item-specific memory. *Neuropsychiatr Dis Treat* 12, 1157–1166. 10.2147/NDT.S104384. [PubMed: 27274250]
- Junyent F, and Kremer EJ (2015). CAV-2--why a canine virus is a neurobiologist's best friend. *Curr Opin Pharmacol* 24, 86–93. 10.1016/j.coph.2015.08.004. [PubMed: 26298516]
- Kalivas PW, Duffy P, and White SR (1998). MDMA elicits behavioral and neurochemical sensitization in rats. *Neuropsychopharmacology* 18, 469–479. 10.1016/S0893-133X(97)00195-4. [PubMed: 9571655]
- Kastellakis G, Silva AJ, and Poirazi P (2016). Linking Memories across Time via Neuronal and Dendritic Overlaps in Model Neurons with Active Dendrites. *Cell reports* 17, 1491–1504. 10.1016/j.celrep.2016.10.015. [PubMed: 27806290]
- Kempadoo KA, Mosharov EV, Choi SJ, Sulzer D, and Kandel ER (2016). Dopamine release from the locus coeruleus to the dorsal hippocampus promotes spatial learning and memory. *Proc Natl Acad Sci U S A* 113, 14835–14840. 10.1073/pnas.1616515114. [PubMed: 27930324]
- Kocsis B, Varga V, Dahan L, and Sik A (2006). Serotonergic neuron diversity: identification of raphe neurons with discharges time-locked to the hippocampal theta rhythm. *Proc Natl Acad Sci U S A* 103, 1059–1064. 10.1073/pnas.0508360103. [PubMed: 16418294]
- Krashes MJ, Koda S, Ye C, Rogan SC, Adams AC, Cusher DS, Maratos-Flier E, Roth BL, and Lowell BB (2011). Rapid, reversible activation of AgRP neurons drives feeding behavior in mice. *The Journal of clinical investigation* 121, 1424–1428. 10.1172/JCI46229. [PubMed: 21364278]
- Lammel S, Ion DI, Roeper J, and Malenka RC (2011). Projection-specific modulation of dopamine neuron synapses by aversive and rewarding stimuli. *Neuron* 70, 855–862. 10.1016/j.neuron.2011.03.025. [PubMed: 21658580]
- Lemon N, and Manahan-Vaughan D (2006). Dopamine D1/D5 receptors gate the acquisition of novel information through hippocampal long-term potentiation and long-term depression. *The Journal of neuroscience : the official journal of the Society for Neuroscience* 26, 7723–7729. 10.1523/JNEUROSCI.1454-06.2006.
- Li S, Cullen WK, Anwyl R, and Rowan MJ (2003). Dopamine-dependent facilitation of LTP induction in hippocampal CA1 by exposure to spatial novelty. *Nature neuroscience* 6, 526–531. 10.1038/nn1049. [PubMed: 12704392]
- Likhtik E, and Johansen JP (2019). Neuromodulation in circuits of aversive emotional learning. *Nature neuroscience* 22, 1586–1597. 10.1038/s41593-019-0503-3. [PubMed: 31551602]
- Lisman JE, and Grace AA (2005). The hippocampal-VTA loop: controlling the entry of information into long-term memory. *Neuron* 46, 703–713. 10.1016/j.neuron.2005.05.002. [PubMed: 15924857]

- Lopes-dos-Santos V, Ribeiro S, and Tort AB (2013). Detecting cell assemblies in large neuronal populations. *J Neurosci Methods* 220, 149–166. 10.1016/j.jneumeth.2013.04.010. [PubMed: 23639919]
- Luchetti A, Bota A, Weitemier A, Mizuta K, Sato M, Islam T, McHugh TJ, Tashiro A, and Hayashi Y (2020). Two Functionally Distinct Serotonergic Projections into Hippocampus. *The Journal of neuroscience : the official journal of the Society for Neuroscience* 40, 4936–4944. 10.1523/JNEUROSCI.2724-19.2020.
- Malenka RC, and Nicoll RA (1986). Dopamine decreases the calcium-activated afterhyperpolarization in hippocampal CA1 pyramidal cells. *Brain Res* 379, 210–215. 10.1016/0006-8993(86)90773-0. [PubMed: 3017510]
- Mankin EA, Sparks FT, Slayyeh B, Sutherland RJ, Leutgeb S, and Leutgeb JK (2012). Neuronal code for extended time in the hippocampus. *Proc Natl Acad Sci U S A* 109, 19462–19467. 10.1073/pnas.1214107109. [PubMed: 23132944]
- McNamara CG, and Dupret D (2017). Two sources of dopamine for the hippocampus. *Trends Neurosci* 40, 383–384. 10.1016/j.tins.2017.05.005. [PubMed: 28511793]
- McNamara CG, Tejero-Cantero A, Trouche S, Campo-Urriza N, and Dupret D (2014). Dopaminergic neurons promote hippocampal reactivation and spatial memory persistence. *Nature neuroscience* 17, 1658–1660. 10.1038/nn.3843. [PubMed: 25326690]
- Mizuseki K, and Buzsaki G (2014). Theta oscillations decrease spike synchrony in the hippocampus and entorhinal cortex. *Philos Trans R Soc Lond B Biol Sci* 369, 20120530. 10.1098/rstb.2012.0530.
- Molitor RJ, Sherrill KR, Morton NW, Miller AA, and Preston AR (2021). Memory Reactivation during Learning Simultaneously Promotes Dentate Gyrus/CA2,3 Pattern Differentiation and CA1 Memory Integration. *The Journal of neuroscience : the official journal of the Society for Neuroscience* 41, 726–738. 10.1523/JNEUROSCI.0394-20.2020. [PubMed: 33239402]
- Moyer JR Jr., Thompson LT, and Disterhoft JF (1996). Trace eyeblink conditioning increases CA1 excitability in a transient and learning-specific manner. *The Journal of neuroscience : the official journal of the Society for Neuroscience* 16, 5536–5546. [PubMed: 8757265]
- Nemeth VL, Csete G, Drotos G, Greminger N, Janka Z, Vecsei L, and Must A (2016). The Effect of Emotion and Reward Contingencies on Relational Memory in Major Depression: An Eye-Movement Study with Follow-Up. *Front Psychol* 7, 1849. 10.3389/fpsyg.2016.01849. [PubMed: 27920752]
- Oh MM, and Disterhoft JF (2020). Learning and aging affect neuronal excitability and learning. *Neurobiol Learn Mem* 167, 107133. 10.1016/j.nlm.2019.107133.
- Oh MM, Oliveira FA, and Disterhoft JF (2010). Learning and aging related changes in intrinsic neuronal excitability. *Frontiers in aging neuroscience* 2, 2. 10.3389/neuro.24.002.2010. [PubMed: 20552042]
- Otmakhova NA, and Lisman JE (1996). D1/D5 dopamine receptor activation increases the magnitude of early long-term potentiation at CA1 hippocampal synapses. *The Journal of neuroscience : the official journal of the Society for Neuroscience* 16, 7478–7486. [PubMed: 8922403]
- Palacios-Filardo J, and Mellor JR (2019). Neuromodulation of hippocampal long-term synaptic plasticity. *Curr Opin Neurobiol* 54, 37–43. 10.1016/j.conb.2018.08.009. [PubMed: 30212713]
- Pedarzani P, and Storm JF (1995). Dopamine modulates the slow Ca(2+)-activated K⁺ current IAHP via cyclic AMP-dependent protein kinase in hippocampal neurons. *Journal of neurophysiology* 74, 2749–2753. 10.1152/jn.1995.74.6.2749. [PubMed: 8747230]
- Perez-Escudero A, Vicente-Page J, Hinz RC, Arganda S, and de Polavieja GG (2014). idTracker: tracking individuals in a group by automatic identification of unmarked animals. *Nature methods* 11, 743–748. 10.1038/nmeth.2994. [PubMed: 24880877]
- Pnevmatikakis EA, and Giovannucci A (2017). NoRMCorre: An online algorithm for piecewise rigid motion correction of calcium imaging data. *Journal of neuroscience methods* 291, 83–94. 10.1016/j.jneumeth.2017.07.031. [PubMed: 28782629]
- Poe GR, Foote S, Eschenko O, Johansen JP, Bouret S, Aston-Jones G, Harley CW, Manahan-Vaughan D, Weinshenker D, Valentino R, et al. (2020). Locus coeruleus: a new look at the blue spot. *Nat Rev Neurosci* 21, 644–659. 10.1038/s41583-020-0360-9. [PubMed: 32943779]

- Ranjbar-Slamloo Y, and Fazlali Z (2019). Dopamine and Noradrenaline in the Brain; Overlapping or Dissociate Functions? *Front Mol Neurosci* 12, 334. 10.3389/fnmol.2019.00334. [PubMed: 32038164]
- Rashid AJ, Yan C, Mercaldo V, Hsiang HL, Park S, Cole CJ, De Cristofaro A, Yu J, Ramakrishnan C, Lee SY, et al. (2016). Competition between engrams influences fear memory formation and recall. *Science* 353, 383–387. 10.1126/science.aaf0594. [PubMed: 27463673]
- Rossato JI, Bevilacqua LR, Izquierdo I, Medina JH, and Cammarota M (2009). Dopamine controls persistence of long-term memory storage. *Science* 325, 1017–1020. 10.1126/science.1172545. [PubMed: 19696353]
- Sano Y, Shobe JL, Zhou M, Huang S, Shuman T, Cai DJ, Golshani P, Kamata M, and Silva AJ (2014). CREB regulates memory allocation in the insular cortex. *Current biology : CB* 24, 2833–2837. 10.1016/j.cub.2014.10.018. [PubMed: 25454591]
- Schapiro AC, Turk-Browne NB, Botvinick MM, and Norman KA (2017). Complementary learning systems within the hippocampus: a neural network modelling approach to reconciling episodic memory with statistical learning. *Philos Trans R Soc Lond B Biol Sci* 372. 10.1098/rstb.2016.0049.
- Schlichting ML, Zeithamova D, and Preston AR (2014). CA1 subfield contributions to memory integration and inference. *Hippocampus* 24, 1248–1260. 10.1002/hipo.22310. [PubMed: 24888442]
- Shgal M, Ehlers VL, and Moyer JR Jr. (2014). Learning enhances intrinsic excitability in a subset of lateral amygdala neurons. *Learn Mem* 21, 161–170. 10.1101/lm.032730.113. [PubMed: 24554670]
- Shgal M, Zhou M, Lavi A, Huang S, Zhou Y, and Silva AJ (2018). Memory allocation mechanisms underlie memory linking across time. *Neurobiol Learn Mem* 153, 21–25. 10.1016/j.nlm.2018.02.021. [PubMed: 29496645]
- Shohamy D, and Adcock RA (2010). Dopamine and adaptive memory. *Trends in cognitive sciences* 14, 464–472. 10.1016/j.tics.2010.08.002. [PubMed: 20829095]
- Silva AJ, Zhou Y, Rogerson T, Shobe J, and Balaji J (2009). Molecular and cellular approaches to memory allocation in neural circuits. *Science* 326, 391–395. 10.1126/science.1174519. [PubMed: 19833959]
- Smith CC, and Greene RW (2012). CNS dopamine transmission mediated by noradrenergic innervation. *The Journal of neuroscience : the official journal of the Society for Neuroscience* 32, 6072–6080. 10.1523/JNEUROSCI.6486-11.2012. [PubMed: 22553014]
- Sosa M, and Giocomo LM (2021). Navigating for reward. *Nat Rev Neurosci* 22, 472–487. 10.1038/s41583-021-00479-z. [PubMed: 34230644]
- Soudais C, Laplace-Builhe C, Kissa K, and Kremer EJ (2001). Preferential transduction of neurons by canine adenovirus vectors and their efficient retrograde transport in vivo. *FASEB J* 15, 2283–2285. 10.1096/fj.01-0321fje. [PubMed: 11511531]
- Stachniak TJ, Ghosh A, and Sternson SM (2014). Chemogenetic synaptic silencing of neural circuits localizes a hypothalamus-->midbrain pathway for feeding behavior. *Neuron* 82, 797–808. 10.1016/j.neuron.2014.04.008. [PubMed: 24768300]
- Stanzione P, Calabresi P, Mercuri N, and Bernardi G (1984). Dopamine modulates CA1 hippocampal neurons by elevating the threshold for spike generation: an in vitro study. *Neuroscience* 13, 1105–1116. 10.1016/0306-4522(84)90291-4. [PubMed: 6527792]
- Strange BA, Hurlmann R, and Dolan RJ (2003). An emotion-induced retrograde amnesia in humans is amygdala- and beta-adrenergic-dependent. *Proc Natl Acad Sci U S A* 100, 13626–13631. 10.1073/pnas.1635116100. [PubMed: 14595032]
- Takeuchi T, Duzsikiewicz AJ, Sonneborn A, Spooner PA, Yamasaki M, Watanabe M, Smith CC, Fernandez G, Deisseroth K, Greene RW, and Morris RG (2016). Locus coeruleus and dopaminergic consolidation of everyday memory. *Nature* 537, 357–362. 10.1038/nature19325. [PubMed: 27602521]
- Teissier A, Chemiakine A, Inbar B, Bagchi S, Ray RS, Palmiter RD, Dymecki SM, Moore H, and Ansorge MS (2015). Activity of Raphe Serotonergic Neurons Controls Emotional Behaviors. *Cell reports* 13, 1965–1976. 10.1016/j.celrep.2015.10.061. [PubMed: 26655908]

- Thiele A, and Bellgrove MA (2018). Neuromodulation of Attention. *Neuron* 97, 769–785. 10.1016/j.neuron.2018.01.008. [PubMed: 29470969]
- Titone D, Ditman T, Holzman PS, Eichenbaum H, and Levy DL (2004). Transitive inference in schizophrenia: impairments in relational memory organization. *Schizophr Res* 68, 235–247. 10.1016/S0920-9964(03)00152-X. [PubMed: 15099606]
- Tzivilivaki A, Kastellakis G, and Poirazi P (2019). Challenging the point neuron dogma: FS basket cells as 2-stage nonlinear integrators. *Nat Commun* 10, 3664. 10.1038/s41467-019-11537-7. [PubMed: 31413258]
- Vanderschuren LJ, Schmidt ED, De Vries TJ, Van Moorsel CA, Tilders FJ, and Schoffelmeer AN (1999). A single exposure to amphetamine is sufficient to induce long-term behavioral, neuroendocrine, and neurochemical sensitization in rats. *The Journal of neuroscience : the official journal of the Society for Neuroscience* 19, 9579–9586. [PubMed: 10531460]
- Varga V, Losonczy A, Zemelman BV, Borhegyi Z, Nyiri G, Domonkos A, Hangya B, Holderith N, Magee JC, and Freund TF (2009). Fast synaptic subcortical control of hippocampal circuits. *Science* 326, 449–453. 10.1126/science.1178307. [PubMed: 19833972]
- Ventura R, Latagliata EC, Morrone C, La Mela I, and Puglisi-Allegra S (2008). Prefrontal norepinephrine determines attribution of “high” motivational salience. *PLoS One* 3, e3044. 10.1371/journal.pone.0003044. [PubMed: 18725944]
- Wagatsuma A, Okuyama T, Sun C, Smith LM, Abe K, and Tonegawa S (2018). Locus coeruleus input to hippocampal CA3 drives single-trial learning of a novel context. *Proc Natl Acad Sci U S A* 115, E310–E316. 10.1073/pnas.1714082115. [PubMed: 29279390]
- Yokose J, Okubo-Suzuki R, Nomoto M, Ohkawa N, Nishizono H, Suzuki A, Matsuo M, Tsujimura S, Takahashi Y, Nagase M, et al. (2017). Overlapping memory trace indispensable for linking, but not recalling, individual memories. *Science* 355, 398–403. 10.1126/science.aal2690. [PubMed: 28126819]
- Zhou P, Resendez SL, Rodriguez-Romaguera J, Jimenez JC, Neufeld SQ, Giovannucci A, Friedrich J, Pnevmatikakis EA, Stuber GD, Hen R, et al. (2018). Efficient and accurate extraction of in vivo calcium signals from microendoscopic video data. *eLife* 7. 10.7554/eLife.28728.
- Zhou Y, Won J, Karlsson MG, Zhou M, Rogerson T, Balaji J, Neve R, Poirazi P, and Silva AJ (2009). CREB regulates excitability and the allocation of memory to subsets of neurons in the amygdala. *Nature neuroscience* 12, 1438–1443. 10.1038/nn.2405. [PubMed: 19783993]
- Ziv Y, Burns LD, Cocker ED, Hamel EO, Ghosh KK, Kitch LJ, El Gamal A, and Schnitzer MJ (2013). Long-term dynamics of CA1 hippocampal place codes. *Nature neuroscience* 16, 264–266. 10.1038/nn.3329. [PubMed: 23396101]

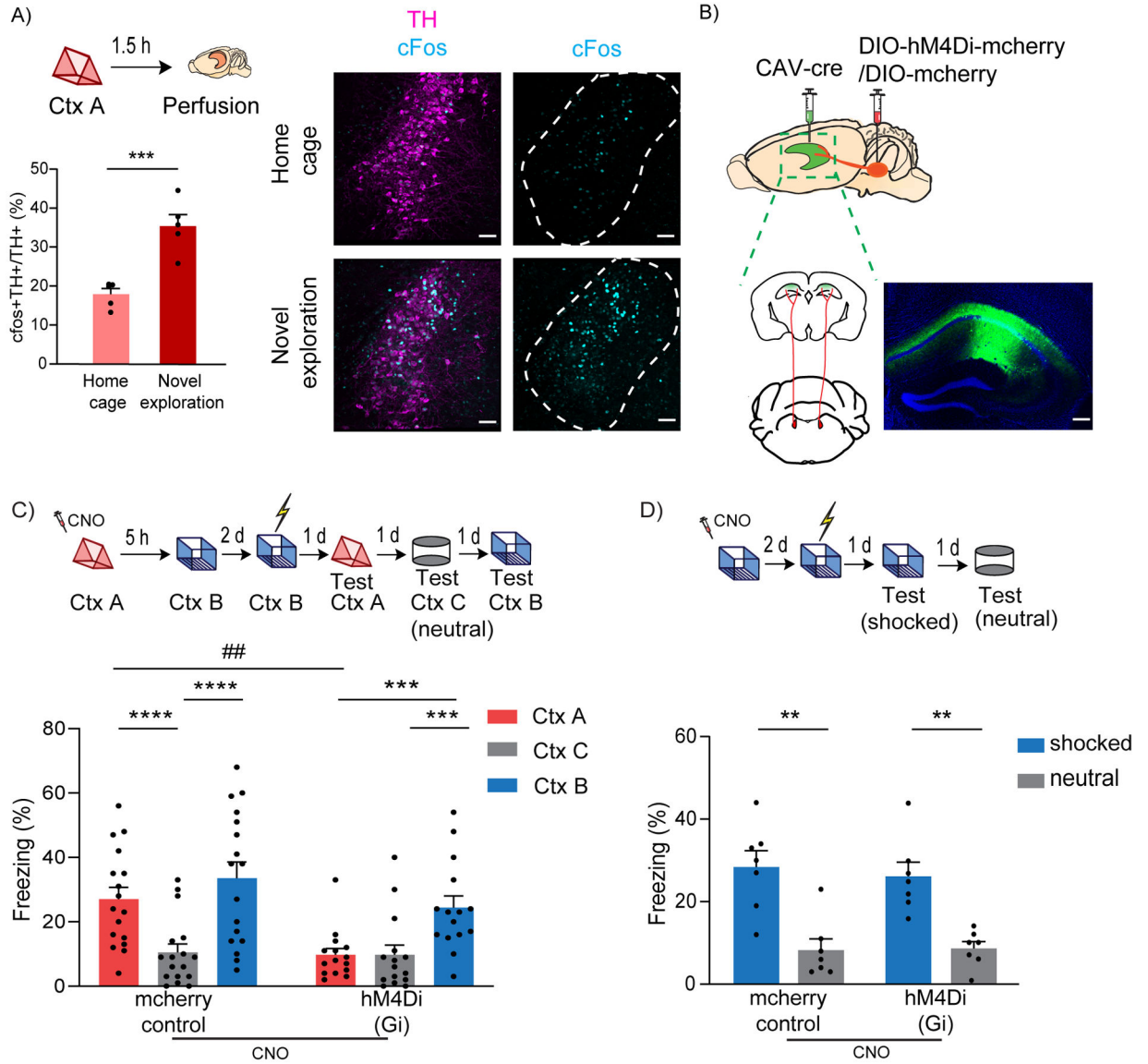


Figure 1: LC to dCA1 projecting cells are required for contextual memory linking, but not for contextual conditioning

(A) Exploration of a novel context increased cFos expression in the TH+ cells of LC (unpaired t-test, n=5, ***p<0.001). Example images of TH and cFos staining in LC. Scale bar, 50µm. TH- magenta, cFos- cyan. The LC is outlined.

(B) Schematics of experimental design for surgery. Example image for virus spread in HP estimated with AAV-DIO-GFP injected together with CAV-cre. Scale bar, 300µm.

(C) Inhibition of LC cells projecting to dCA1 during exploration of context A impaired contextual memory linking tested with a 5 hours interval. (Control, n=17; LC inhibited, n=15. Two-way repeated measures ANOVA, Sidak post hoc. ##p <0.01, ***p<0.001, ****p<0.0001). Context A- Ctx A, Context B- Ctx B, Context C- Ctx C (neutral). CNO- Clozapine-N-oxide was given to all mice. * is used to depict significance within groups and # is used to show significance between groups for two-way RM ANOVA.

(D) Inhibition of LC cells projecting to dCA1 did not affect contextual conditioning (Two-way RM ANOVA, Sidak posthoc test; control, n=7; LC inhibited, n=7, **p<0.001). CNO-Clozapine-N-oxide was given to all mice.

All results are mean \pm s.e.m.

Author Manuscript

Author Manuscript

Author Manuscript

Author Manuscript

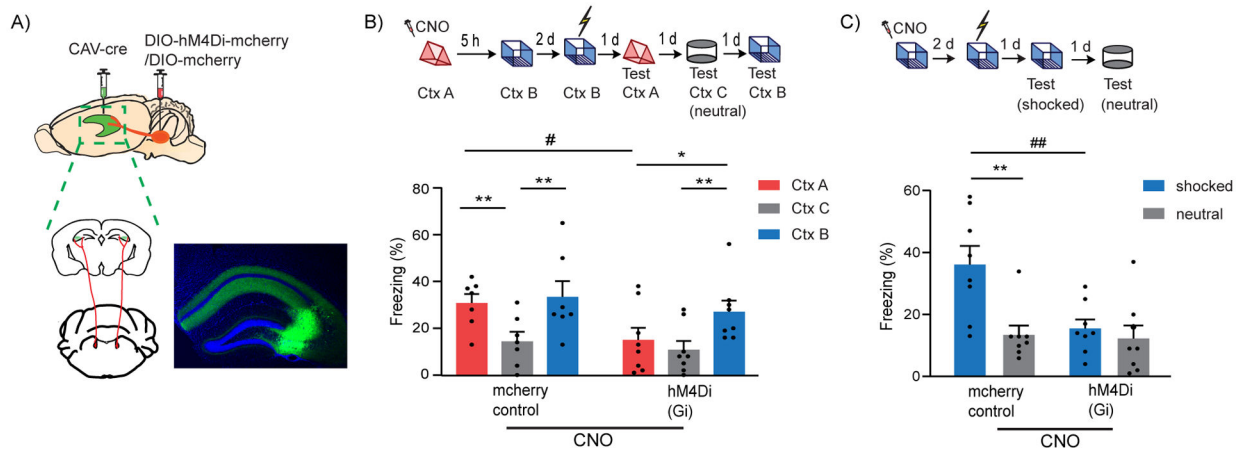


Figure 2: LC to dCA3 projecting cells are required for contextual memory formation

(A) Schematics of experimental design for surgery. Example image for virus spread in HP estimated with AAV-DIO-GFP injected together with CAV-cre. Scale bar, 300 μ m.

(B) Inhibition of LC cells projecting to dCA3 during exploration of context A impaired performance in contextual memory linking tested with a 5 hours interval. (Control, n=7; LC inhibited, n=8. Two-way repeated measures ANOVA, Sidak post hoc. #p < 0.05, *p < 0.05, **p < 0.01). Clozapine-N-oxide was given to all mice. * is used to depict significance within groups and # is used to show significance between groups for two-way RM ANOVA.

(C) Inhibition of LC cells projecting to dCA3 impaired contextual conditioning (control, n=8; LC inhibited, n=8; Two-way RM ANOVA, Sidak posthoc test; **p < 0.001, ##p < 0.01). Clozapine-N-oxide was given to all mice. * is used to depict significance within groups and # is used to show significance between groups for two-way RM ANOVA.

All results are mean \pm s.e.m.

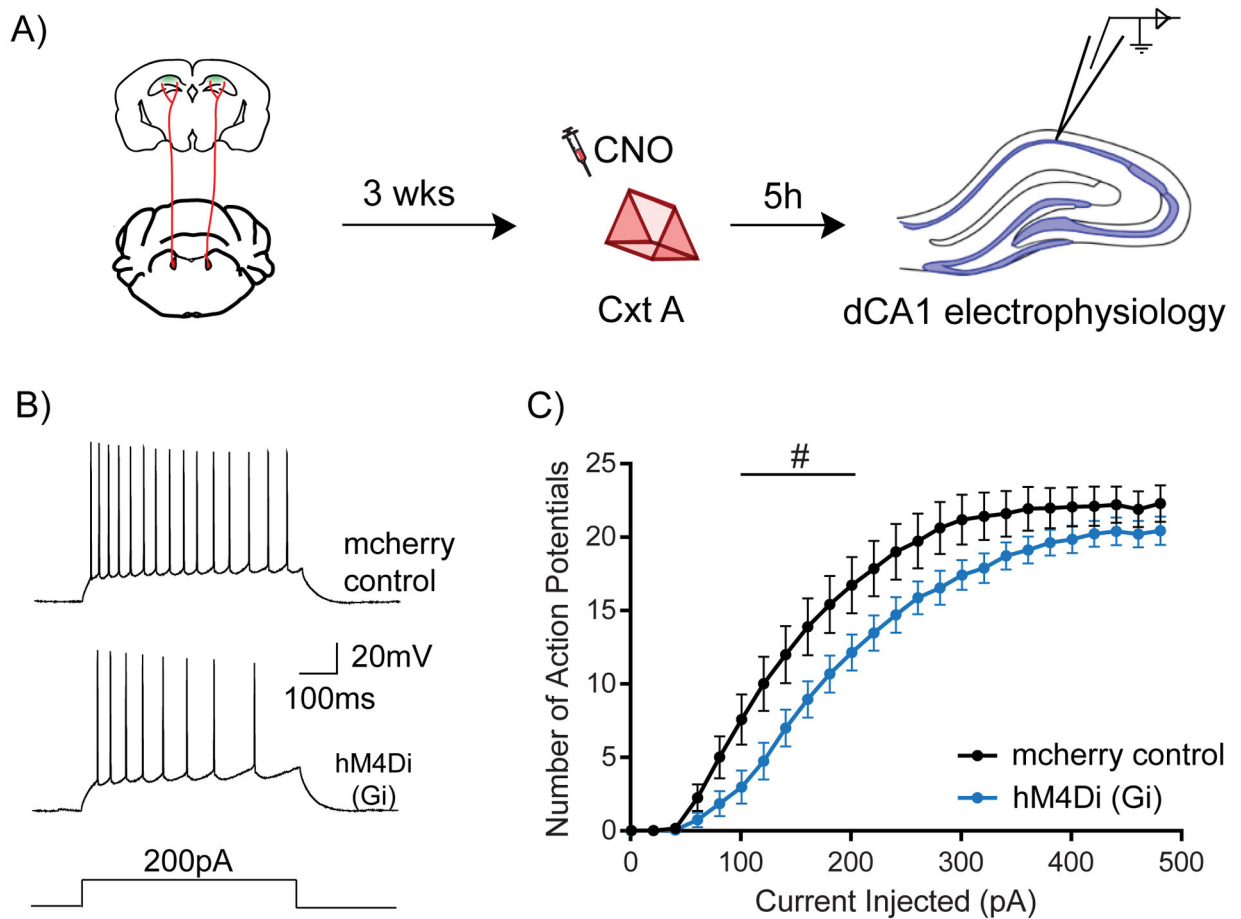


Figure 3: LC to dCA1 inhibition decreases novelty induced increases in neuronal excitability

(A) Experimental design for measuring dCA1 neuronal excitability.

(B) Representative traces showing adaptive firing responses to a 200pA current injection in dCA1 pyramidal neurons.

(C) Inhibition of LC cells projecting to dCA1 during context exploration reduced the firing rate of dCA1 neurons 5 hours later (Two-way repeated measures ANOVA; control n=15, LC inhibited n=15, #p<0.05). Clozapine-N-oxide was given to all mice. # is used to show significance between groups for two-way RM ANOVA.

All results are mean + s.e.m.

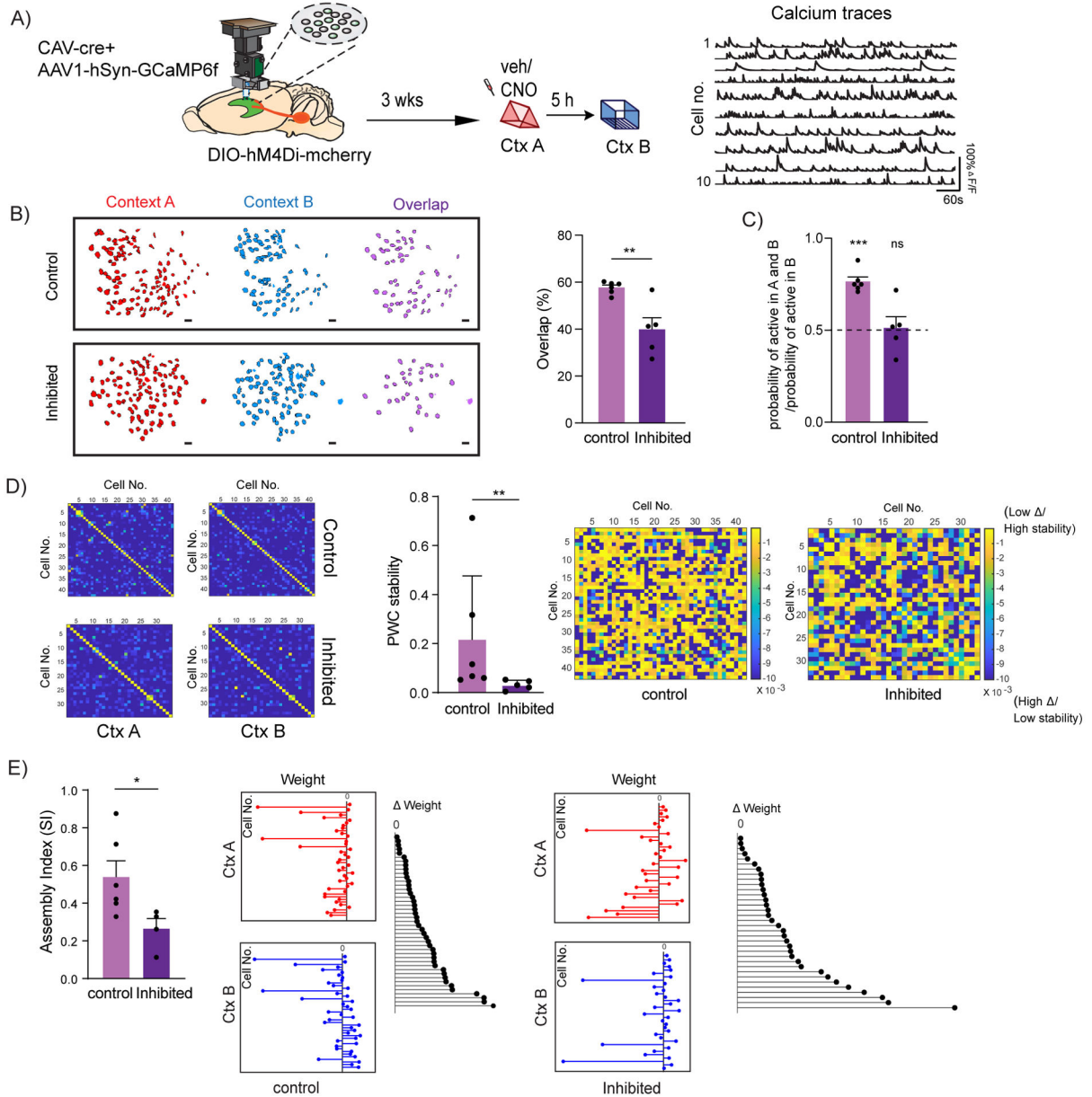


Figure 4: LC to dCA1 inhibition decreases the overlap between dCA1 memory ensembles and affects their firing properties

(A) Schematics for miniscope setup and calcium signal imaging in dCA1. Example calcium traces.

(B) Inhibition of LC neurons projecting to dCA1 reduced the percentage overlap between memory ensembles encoding contexts explored 5 hours apart (Control n=6, and LC inhibited n=5; unpaired t-test, **p<0.01). Percentage overlap was calculated as neurons active in both A and B over total cells active in A and B. Example plots of active neurons in contexts A and B and neuronal overlap between different conditions. Scale bars, 50 μm.

(C) Inhibition of LC neurons projecting to dCA1 reduced the likelihood to chance levels (dashed line) that a cell active in context B had previously been active in context A (Control n=6, and LC inhibited n=5; One-sample t-test over 0.5 as chance level, ***p< 0.001).

(D) Within the overlapping neuronal population, inhibition of the LC neurons projecting to dCA1 reduced the stability of the coactivity maps between the two contexts visited (Control n=6, and LC inhibited n=5; Mann Whitney test, $**p<0.01$). Example PWC stability maps.

(E) Inhibition of the LC neurons projecting to dCA1 reduced the stability of the dCA1 assemblies detected within the overlapping neuronal population (Control n=6, and LC inhibited n=4; unpaired t-test, $*p<0.05$). Representative images for weight distribution of the assemblies detected for context A (red), context B (blue), or delta between the two weights (black) with all neurons sorted in the same order in all 3 graphs.

All results are mean + s.e.m.

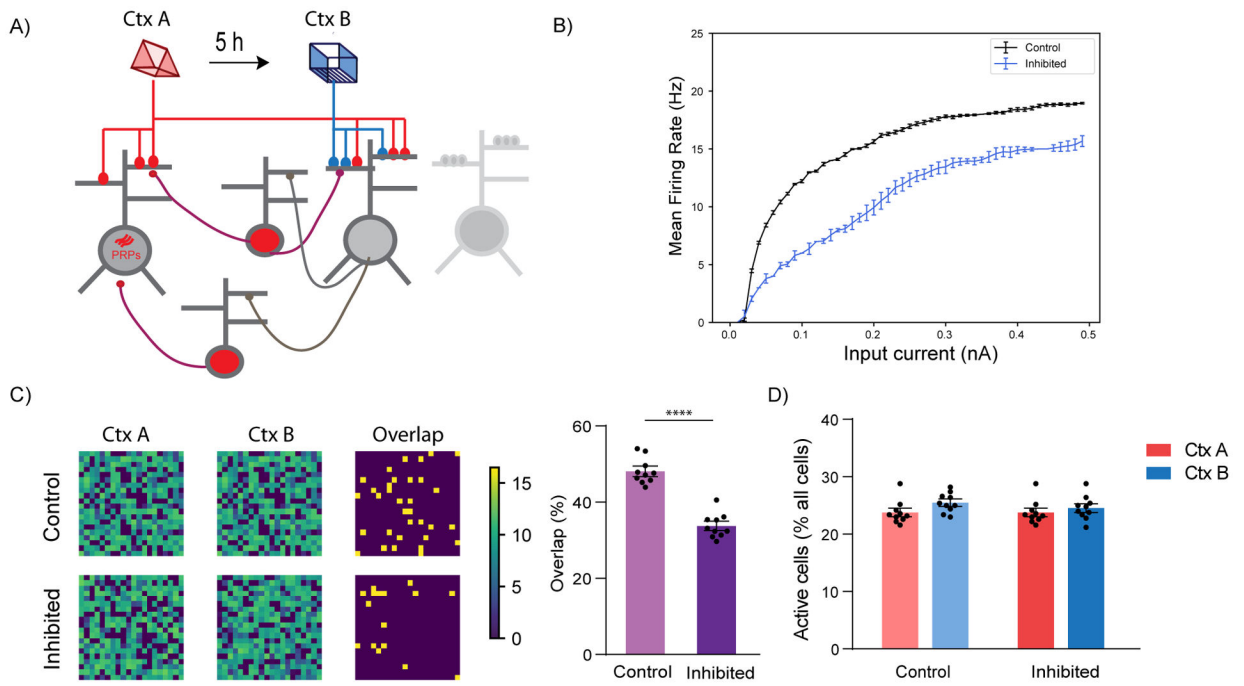


Figure 5: Simulation of LC to dCA1 inhibition using a spiking network model

(A) Conceptual diagram of the spiking network model. The model includes excitatory neurons (gray) and subpopulations of interneurons (red). Synaptic inputs representing different memories terminate in overlapping dendrites. Two novel contexts are simulated as memories A and B, separated by 5h.

(B) Firing rate of neurons when current input is applied directly to the somatic compartment of the 2-stage neurons under control (blue) and LC inhibition (orange) condition. Under conditions of LC blocking, the excitability of the neurons does not increase, $n=50$.

(C) Simulation of LC to dCA1 inhibition resulted in a reduction of the overlapping neuronal population. Percentage overlap was calculated as neurons activated during both context A and B over the total active neurons in A and B. $n=10$ simulation trials, unpaired t-test, **** $p<0.0001$. The contour plots show population activation during encoding of memories in context A and B. The third column indicates the neurons which were active ($ff > 10\text{Hz}$) during both memories.

(D) The sizes of activated populations (number of neurons with $ff > 10\text{Hz}$) during the encoding of Ctx A and Ctx B, under different conditions.

All results are mean + s.e.m.

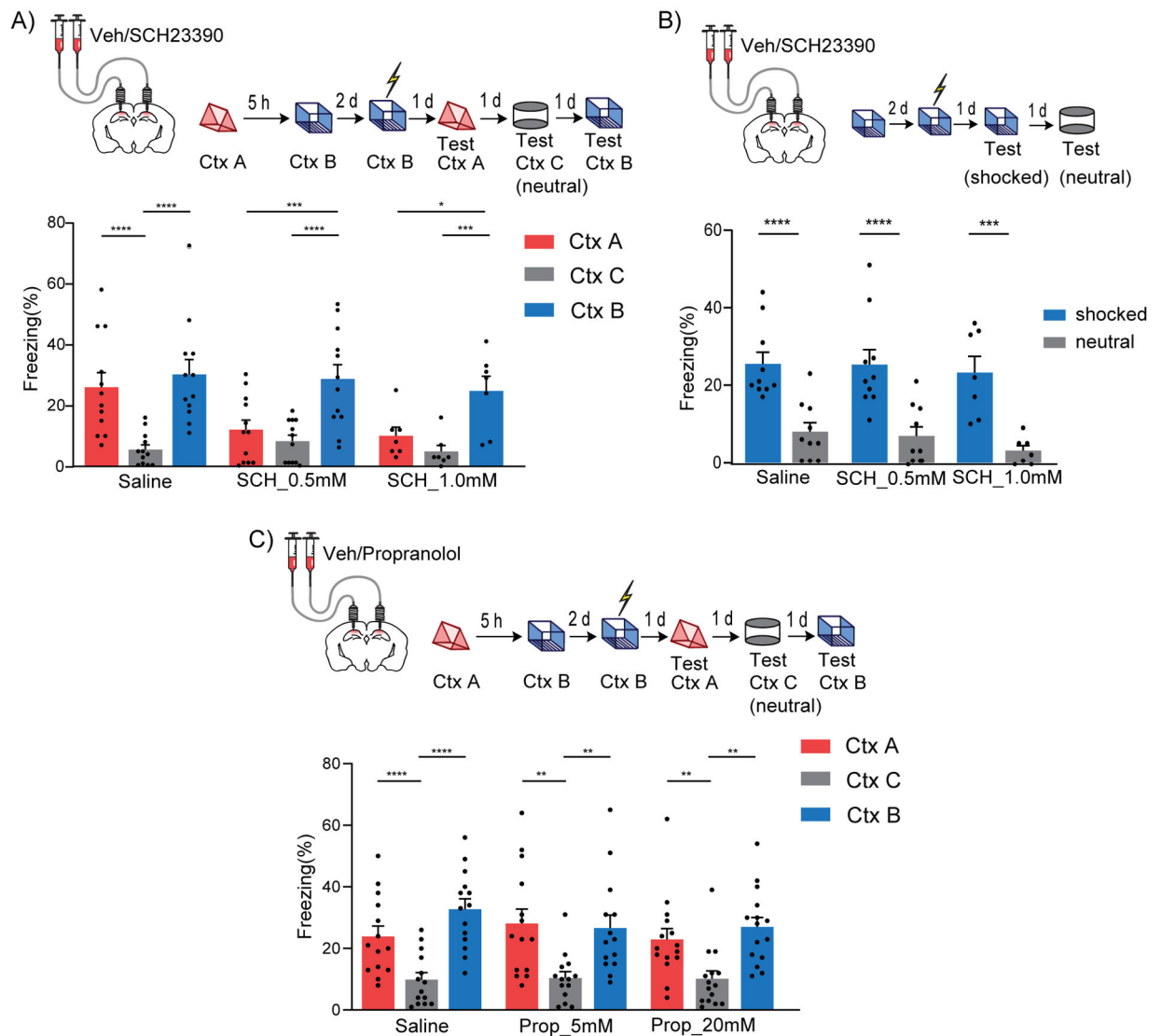


Figure 6: Dopamine D1/D5 receptors in dCA1 modulate contextual memory linking

(A) Inhibition of Dopamine D1/D5 receptors in dCA1 during context A disrupted contextual memory linking. (Saline, n=12; SCH 0.5 mM, n=12; SCH 1.0 mM, n=7; two-way repeated measures ANOVA, Sidak post hoc, *p<0.05, **p<0.01, ***p<0.001, ****p<0.0001)

(B) Inhibition of Dopamine D1/D5 receptors in dCA1 did not affect contextual memory formation at the doses used. (Saline, n=10; SCH 0.5 mM, n=10; SCH 1.0 mM, n=7; two-way repeated measures ANOVA, Sidak post hoc, ***p<0.001, ****p<0.0001).

(C) Inhibition of β -adrenergic receptors in dCA1 did not affect contextual memory linking at the doses used. (Saline, n=14; Prop 5 mM, n=14; Prop 20 mM, n=15; two-way repeated measures ANOVA, Sidak post hoc, **p<0.01, ****p<0.0001)

All results are mean + s.e.m.

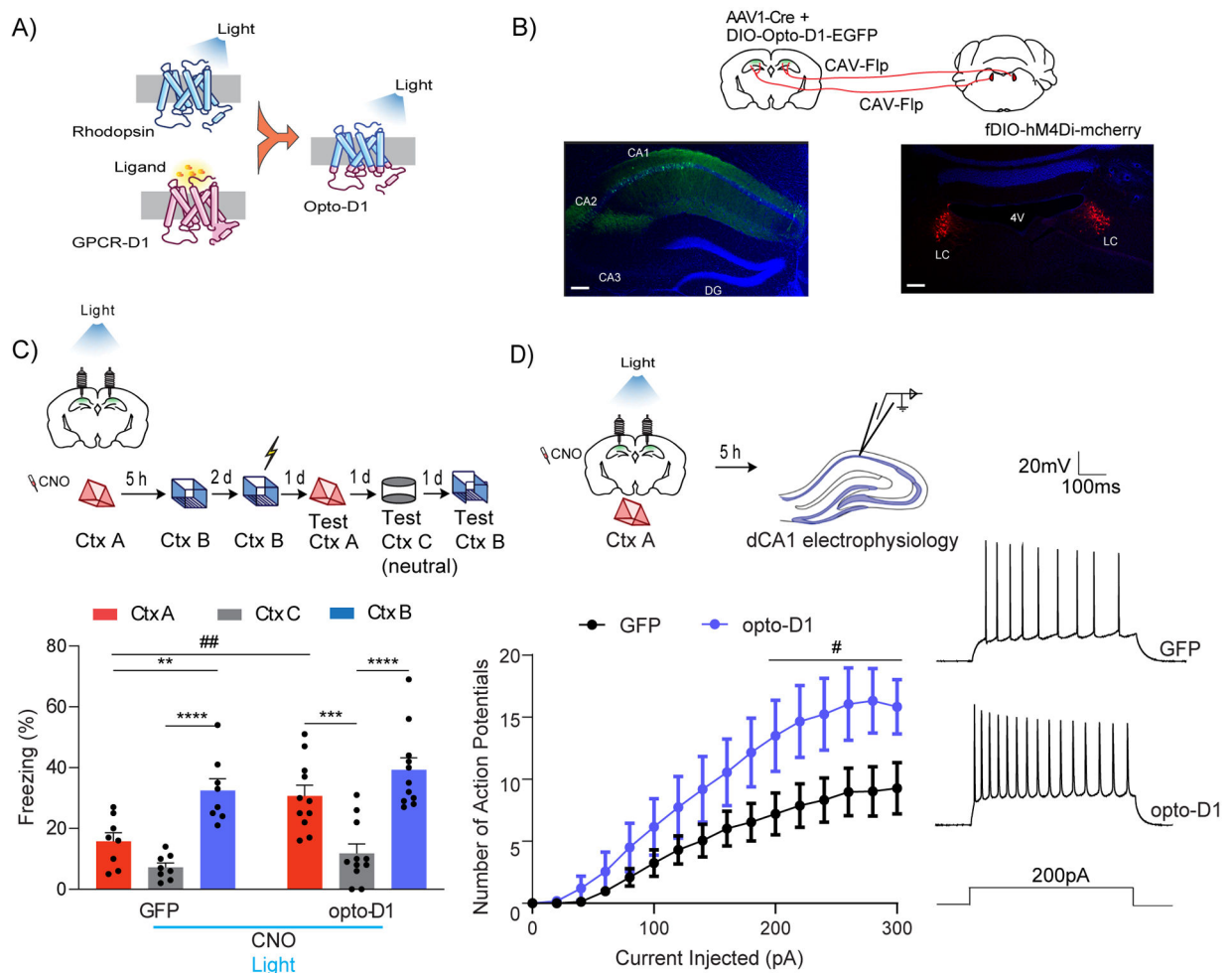


Figure 7: Optogenetic D1 receptor activation in dCA1 rescues linking deficits caused by LC to dCA1 inhibition

(A) Schematics of the Opto-D1 construct.

(B) Schematics of experimental design. Scale bars, 300 μ m.

(C) Optogenetic activation of D1 receptor signaling in a fraction of all cell types in dCA1 rescued the contextual memory linking deficit caused by chemogenetic inhibition of LC cells projecting to dCA1. (GFP, n=8; opto-D1, n=11; two-way repeated measures ANOVA, Sidak post hoc, *p<0.05, **p<0.01, ***p<0.001, ****p<0.0001, ##p<0.01). * is used to depict significance within groups and # is used to show significance between groups for two-way RM ANOVA. Clozapine-N-oxide and light were given to all mice.

(D) Optogenetic activation of the D1 receptor during context exploration rescued the reduction in dCA1 firing rate caused by chemogenetic inhibition of LC cells projecting to the dCA1. (GFP, n=11; opto-D1, n=10; two-way repeated measures ANOVA, factor: D1 activation $F_{(1,19)} = 4.50$, #p<0.05). Clozapine-N-oxide and light were given to all mice. All results are mean + s.e.m.

Key resources table

REAGENT or RESOURCE	SOURCE	IDENTIFIER
Antibodies		
Anti-cFos (rabbit)	Cell Signalling	Cat#2250, RRID: AB_2247211
Anti-GFP (chicken)	Abcam	Cat#AB13970, RRID: AB_300798
Anti-TH (chicken)	Abcam	Cat#AB76442, RRID: AB_1524535
Anti-RFP (rabbit)	Rockland Antibodies	Cat#600-401-379, RRID: AB_2209751
Anti-RFP (guinea pig)	Synaptic Systems	Cat# 390 004, RRID: AB_2737052
Anti-Serotonin transporter (rabbit)	Millipore Sigma	Cat#AB9726, RRID: AB_612176
Bacterial and virus strains		
CAV-cre	Plateforme de Vectorologie de Montpellier, IGMM (Soudais et al., 2001)	Cat# CAV2-cre
CAV2-Flp	Plateforme de Vectorologie de Montpellier, IGMM	Cat# CAV2-Flp
AAV8-hSyn-DIO-hM4D(Gi)-mCherry	Addgene (Krashes et al., 2011)	RRID:Addgene_44362
AAV8-hSyn-DIO-mCherry	Addgene	RRID:Addgene_50459
AAV1. Syn.GCaMP6f.WPRE.SV40	Addgene (Chen et al., 2013)	RRID: Addgene_100837
AAV8-hSyn-DIO-EGFP	Addgene	RRID: Addgene_50457
AAV8- Ef1a-fDIO DREADD Gi-mCherry	Neuroscience Gene Vector and Virus Core at Stanford	Cat#GVVC-AAV-171
AAV8-Ef1a-fDIO-mCherry-WPRE	Neuroscience Gene Vector and Virus Core at Stanford	Cat#GVVC-AAV-155
AAV1-Ef1a-fDIO EYFP	Addgene (Fenno et al., 2014)	RRID:Addgene_55641
AAV1.hSyn.Cre.WPRE.hGH	Addgene	RRID:Addgene_105553
AAV-EF1a-DIO-eArch3.0-EYFP	UNC vector core	N/A
AAV5-EF1a-DIO-OptoD1-EYFP	UNC vector core (Gunaydin et al., 2014)	N/A
AAV-9/2-HSYN 1-CHL-DLOX-M TAGBFP_2A_HM4D(GI_RNRX1B(REV)-DLOX-WPRE-SV40	University of Zurich (Stachniak et al., 2014, Doron et al., 2020)	Cat# v557-9
Chemicals, peptides, and recombinant proteins		
Clozapine-N-Oxide	Tocris	Cat#4936
Super-glue	Loctite	Cat#45198
Dental Cement	Lang Dental	Cat#1223CLR
C&B Metabond Quick Adhesive	Parkell Inc.	Cat#S380
SCH23390	Tocris	Cat#0925
Propranolol	Tocris	Cat#0624
Green and Red Retrobeads™ IX	Lumafuor Inc.	SKU: XN-GRN-RTR-IX SKU: XN-RED-RTR-IX
Deposited data		
Computational Model	Kastellakis et al., 2016	ModelDB database Accession Number 267173
Raw data of quantifications	This paper Main and supplemental figures	Chowdhury, Ananya (2021), "A Locus Coeruleus- dorsal CA1 dopaminergic circuit modulates memory linking. Chowdhury et

REAGENT or RESOURCE	SOURCE	IDENTIFIER
		al.", Mendeley Data, V1, doi: 10.17632/mrk7355wtk.1
Experimental models: Organisms/strains		
Black 6 Wild type	Taconic Farms	C57BL/6NTac
TH-cre	Jackson laboratories	JAX:8601, strain name: B6.Cg-Tg(TH-Cre)1Tmd/J)
Software and algorithms		
MATLAB 2017	Mathworks	https://www.mathworks.com/
Automated Freezing	Med Associates INC (Video Freeze [®] Software)	https://www.med-associates.com/product/video-fear-conditioning/
Imaris 9.2.0	Bitplane AG	www.bitplane.com/imaris/imaris
Prism 9.0.2	GraphPad Software, La Jolla	https://www.graphpad.com/scientific-software/prism/
pClamp 10 software	Molecular Devices	https://www.moleculardevices.com/products/axon-patch-clamp-system/acquisition-and-analysis-software/pclamp-software-suite
Stimfit 0.15.8	(Guzman, et. al, 2014)	https://github.com/neurodroid/stimfit
NoRMCorre	Pnevmatikakis and Giovannucci, 2017	https://github.com/flatironinstitute/NoRMCorre
CNMF-E	Zhou et. al, 2018	https://github.com/zhoupe/CNMF-E
ConcatMiniscope Pipeline	https://doi.org/10.5281/zenodo.5676164	https://github.com/Almeida-FilhoDG/ConcatMiniscope
iDTracker	(Perez-Escudero et al., 2014)	http://www.idtracker.es/
Other		
Microendoscope	UCLA Miniscope	http://miniscope.org
Nanoject II	Fisher Scientific	Cat#13 681 455
Nanoject Controller	World Precision Instrument	Cat#SYS-MICRO4
Guide Cannula	Plastics One	Cat#C313GS-5/SPC
Internal Cannula	Plastics One	C313IS-5/SPC
Fiber Optic Cannula	Newdoon Inc.	Model#FOC-W-1.25-200-0.37-3.0
Grin lens	Edmund Optics	Cat#64-519